Characteristics of Acoustic Propagation to the Eastern Vertical Line Array Receiver During the Summer 1996 New England Shelfbreak PRIMER Experiment

Brian J. Sperry, James F. Lynch, *Senior Member, IEEE*, Glen Gawarkiewicz, Ching-Sang Chiu, and Arthur Newhall

***Abstract*—During July and August of 1996, the summer component of the New England Shelfbreak Front PRIMER Experiment was fielded in the Mid-Atlantic Bight, at a site due south of Martha's Vineyard, MA. This study produced acoustic transmission data from a network of moored sources and receivers in conjunction with very-high-resolution oceanography measurements. This paper analyzes receptions at the northeast array receiver from two 400-Hz acoustic tomography sources, with the transmission paths going from the continental slope onto the continental shelf. These data, along with forward acoustic-propagation modeling based on moored oceanographic data, SeaSoar hydrography measurements, and bottom measurements, reveal many new and interesting aspects of acoustic propagation in a complicated slope-shelf environment. For example, one sees that both the shelfbreak front and tidally generated soliton internal wave packets produce stronger mode coupling than previously expected, leading to an interesting time-and-range-variable population of the acoustic normal modes. Additionally, the arrival time wander and the signal spread of acoustic pulses show variability that can be attributed to the presence of a frontal meander and variability in the soliton field. These and other effects are discussed in this paper, with an emphasis on creating a strong connection between the environmental measurements and the acoustic field characteristics.**

***Index Terms*—PRIMER experiment, shallow-water acoustics, shelfbreak front.**

I. Introduction and Background

THE propagation of acoustic energy in shallow water is often considered to be most strongly characterized by its interactions with the sea bottom and the sea surface boundaries. In many geographic locations, however, the medium between the two boundaries (the watercolumn) can influence the propagating acoustic field just as much as, or even more than, the boundaries themselves, and not just by influencing the interaction with those boundaries. One such location is the continental shelfbreak of the Mid-Atlantic Bight (MAB), which is off the eastern coast of the United States, where large variations in both the bottom topography and the oceanography create a complicated acoustic-propagation environment. The Office of Naval Research's (ONR) Shelfbreak PRIMER program was initiated to look at the both the physical oceanography of the New England shelfbreak front and the characteristics of acoustic propagation through this interesting region.

The motivation for the PRIMER experiment came primarily from two previous efforts investigating propagation in complicated coastal environments: the 1992 Barents Sea Polar Front (BSPF) experiment [1] and the 1995 shallow-water acoustic random media (SWARM) experiment [2]. The BSPF work examined acoustic propagation through a well-measured coastal front, as well as provided some interesting data on acoustic/internal wave (IW) interactions [3], [4]. The 1995 SWARM experiment looked at shallow-water propagation through coastal nonlinear IWs [5]–[7] at a site just south of the Shelfbreak PRIMER location. This experiment also brought extensive acoustic and oceanographic instrumentation together into a single experiment. These two experiments, BSPF and SWARM, featured a shelf front and IWs, respectively. In the PRIMER experiment, we will be looking at a region that is strongly influenced by both phenomena.

There were actually three Shelfbreak PRIMER experiments in all—the spring, summer, and winter seasonal components. Acoustic data were collected only for the latter two seasons; this paper focuses solely on the summer experiment. For readers interested in the other seasons, [8] presents a collection of propagation simulations that cover all three seasons. The overall PRIMER experimental goals were to study both the range of temporal variability (minutes to seasonal) and the spatial variability (meters to tens of kilometers) in the oceanographic and acoustic fields. Due to the large amount of acoustic and oceanographic data collected, this paper only considers the acoustic-propagation characteristics along the eastern edge of the PRIMER experiment study area. The balance of the acoustic data will be considered in forthcoming papers.

To study the oceanography and acoustic propagation, a large number of measurements were made, many of which are shown in plan view in Fig. 1. These included: 1) an acoustic tomography array with four sources on the continental slope and two vertical line array (VLA) receivers on the continental shelf; 2)

Manuscript received August 20, 2002; revised June 15, 2003. This work was performed under Office of Naval Research (ONR) Grants N00014-98-1-0413, N00014-00-1-0931, and N00014-01-1-0772 as part of the ONR Shelfbreak PRIMER initiative.

B. J. Sperry is with Science Applications International, Corp. (SAIC), McLean, VA 22102 USA.

J. F. Lynch, G. Gawarkiewicz, and A. Newhall are with the Woods Hole Oceanographic Institution, Woods Hole, MA 02543 USA.

C.-S. Chiu is with the Naval Postgraduate School, Monterey, CA 93943 USA.

Digital Object Identifier 10.1109/JOE.2003.819153

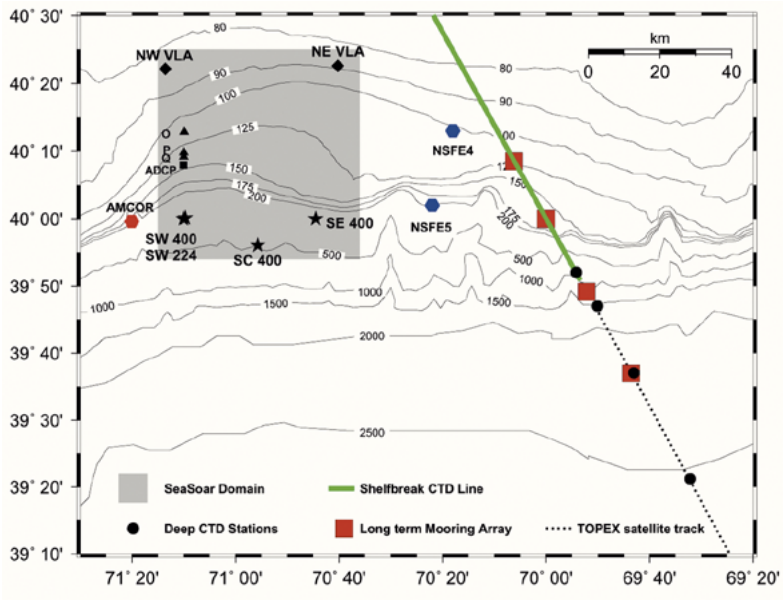

Fig. 1. Summer 1996 shelfbreak PRIMER field study region. The gray-shaded region, denoted "SeaSoar domain," is also the area of intense acoustic measurements.

a number of oceanographic moorings containing thermistors, Sea Cats (temperature and salinity measurement devices), acoustic Doppler and conventional current meters, and pressure sensors; 3) a week-long high resolution hydrography survey with the SeaSoar towed fish sensor (shown in the gray area in Fig. 1); 4) a long-term mooring line to look at the transition from shallow to deep oceanography (not colocated with the other measurements due to fishing-activity considerations); 5) an aircraft- deployed expendable bathythermograph survey of a large area surrounding the SeaSoar box; and 6) cores and a low-frequency acoustic survey to determine bottom geoacoustic parameters. There were other incidental measurements as well, but they will not be pursued here. The details of the primary measurements will be discussed later in this paper.

This paper is organized as follows. In Section II, we discuss the high-resolution oceanographic observations made by both SeaSoar and the moored instrumentation. Section III describes the analysis of a subset of the acoustic data collected at one particular VLA (the northeastern one). Section IV presents a detailed analysis of the acoustic propagation along the eastern edge of the experiment site using parabolic equation and normal mode models, based on the oceanographic measurements described in Section II. Finally, we present conclusions and directions for future studies in Section V.

II. Physical Oceanography Measurements

A sampling of the larger-scale oceanography was provided by SeaSoar, shipboard current profilers, advanced very-high resolution radiometry (AVHRR) satellite data, and two surveys with airborne expendable bathythermographs (AXBTs). Continuous sampling of local meteorological conditions was provided by the ship *R/V Endeavor*. For finer-scale oceanographic sampling, several thermistor chain moorings (labeled "O," "P," and "Q" in Fig. 1), were deployed on the western edge of the site, along with moorings bearing conventional current meters, SeaCats, and an upward-looking acoustic Doppler current profiler (ADCP). Numerous individual thermistors (T-pods) were placed on many of the acoustic moorings as well, providing good coverage in depth and sampling temporally at 1-min sample intervals.

TABLE I
Date to Yearday Conversion for the PRIMER Experiment

Date	7/27	7/28	7/29	7/30	7/31	8/1
Yearday	209	210	211	212	213	214

SeaSoar is essentially a towed conductivity-temperature-depth (CTD) sensor with wings that allow it to be "flown" up and down in the water column while being towed at speeds of up to 8 kn. During the summer experiment, the Woods Hole Oceanographic Institution (WHOI) SeaSoar was deployed from the *R/V Endeavor* for a seven-day period, from July 26 through August 1, 1996. The maximum operating depth was 120 m and the vehicle was not flown closer than 10 m from the bottom. One complete vertical cycle down to 120 m and back required roughly 1 km to complete. The recorded data were averaged and placed onto a standard grid with a resolution of either 1 or 2 km in the horizontal and 2 m in the vertical. The SeaSoar operation plan called for four north–south transects per day, each approximately 50 km long and spaced 10 km apart. Long-line and drift-net fishing activity, however, hindered operations.

A. Physical Oceanographic Features Observed in the PRIMER Region

In the following sections, we describe some of the more important physical oceanographic phenomena, with emphasis on those phenomena that have significant acoustic impact. These include the shelfbreak front, slope eddies and other nearby currents, and the IW field (with emphasis on the nonlinear field).

Because SeaSoar data was only available for a subset of the experiment days, Table I may be useful in relating SeaSoar cov-

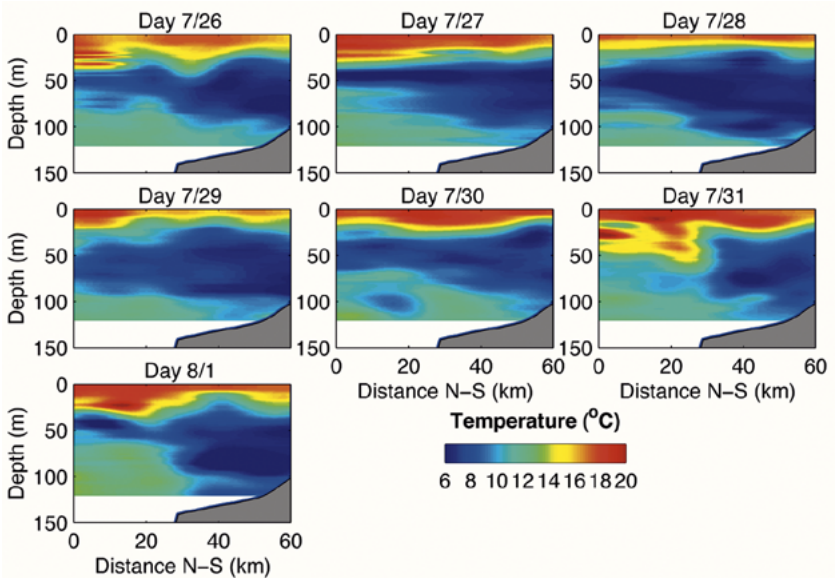

Fig. 2. Raw SeaSoar sections along easternmost track. The range is relative to the location of SE 400-Hz source (40.000 °N, 70.724 °W).

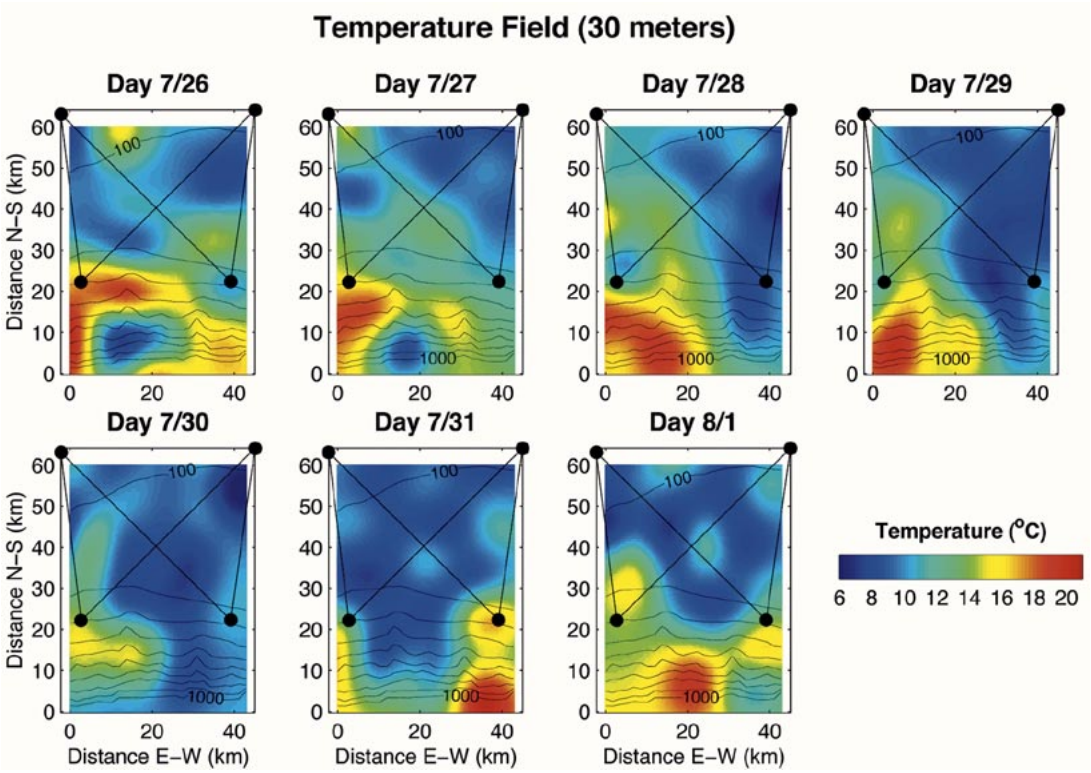

Fig. 3. Temperature map at 30-m depth from SeaSoar.

erage dates to yearday, the latter being used frequently in discussions throughout the paper.

B. Shelfbreak Front

Fig. 2 shows how daily temperature varies with depth in the cross-shelf direction along the easternmost SeaSoar track. These measurements were made once per day at the same time of day and took (roughly) 3 h per track. This easternmost track is of particular interest because it runs nearby and parallel to the acoustic-propagation path from the southeast source (located at range 0 km in the figure) to the northeast VLA receiver. On July 31, a strong downwelling of the warmer surface waters is evident in the temperature field, caused by a frontal meander that strengthened the downwelling cell within the front. Near-surface waters were carried to a depth of 60 m. This feature will be shown to have a very significant acoustic impact. From the week-long SeaSoar records, it appears that, at least along the easternmost section, the front has been pushed well south of the study region, with the exception of days July 31 and August 1, when it reenters from the south after the eastern edge of a

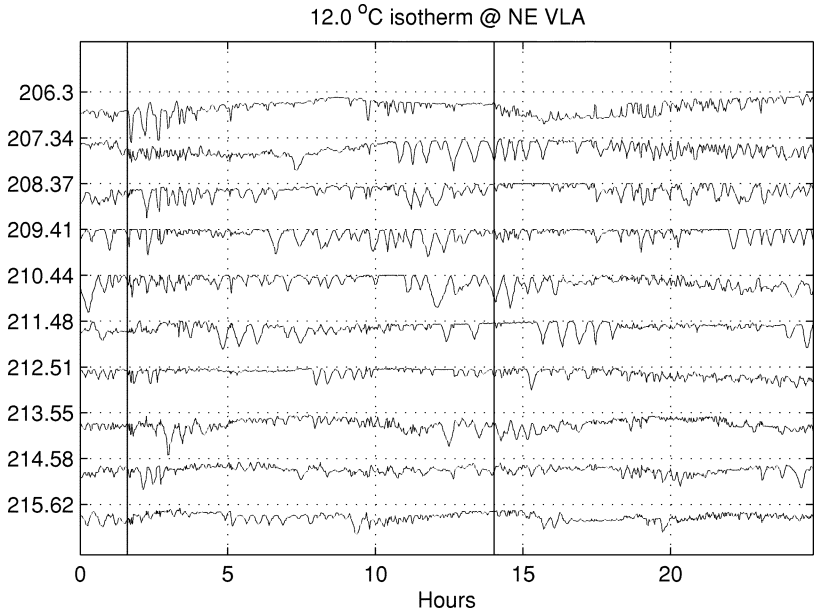

Fig. 4. Vertical displacement of the 12 °C isotherm. Vertical lines represent alignment with a 12.42-h semidiurnal cycle. Offset between isotherm segments is 40 m. Numbers along the y-axis represent starting times for each isotherm in yeardays.

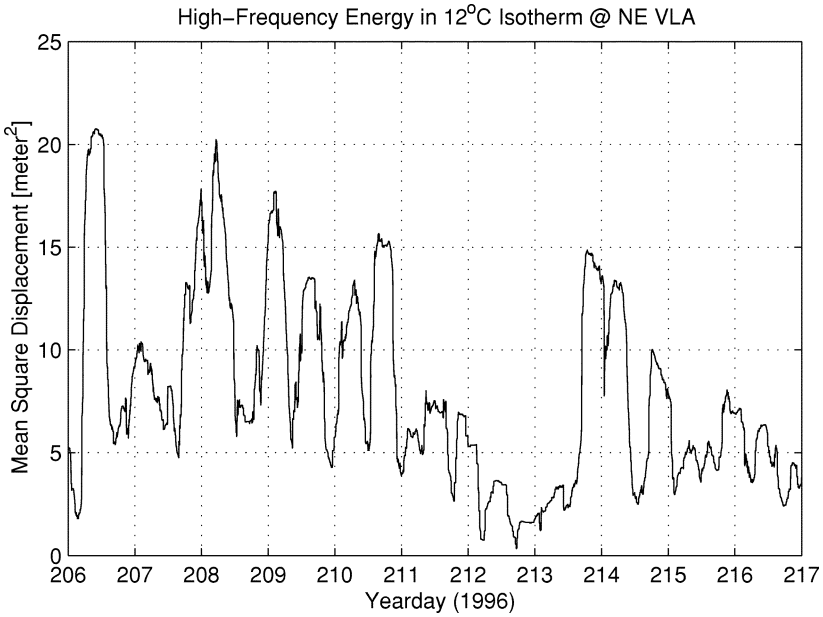

Fig. 5. Estimate of soliton activity at NE VLA, inferred by computing MS highpass-filtered 12 °C isotherm displacement data, using a 4-h sliding-window average.

meander passes to the west. Maximum temperature variability within the frontal region occurs around 30-m depth, where the temperature varies from 5 °C–20 °C. This is consistent with a recent climatology [9]. An important acoustic implication of the strong variability at 30 m is that the lower acoustic modes, which are very sensitive to thermal variations in the sound speed at around 30–40 m depth (just below the mixed layer), will be strongly affected by variations in frontal structure.

Fig. 3 shows a daily plan-view map constructed from objectively analyzed SeaSoar temperature data [a method of three-dimensional (3-D) interpolation] [10]. For reference, the locations of the PRIMER acoustic moorings are indicated. One sees that the shelfbreak front is definitely not a simple, stable feature with distinct boundaries. Rather, it varies from day to day, with significant structure on scales of the baroclinic Rossby radius. Indeed, detailed analysis of the PRIMER oceanography by Gawarkiewicz *et al.* [11] has shown that 10 km is the dominant mesoscale correlation length for the frontal region.

Another prominent feature in the SeaSoar records is a warm more-saline layer of slope water beneath the colder, fresher shelf waters (informally called the “foot” of the shelfbreak front by ocean acousticians). This slope water beneath the front extends onshore to the 100-m isobath, even though the bathymetric shelfbreak is at a 140-m depth; moreover, there can be up to 70 km between the 100- and 140-m isobaths. Like the downwelling cell mentioned earlier, this warm near-bottom

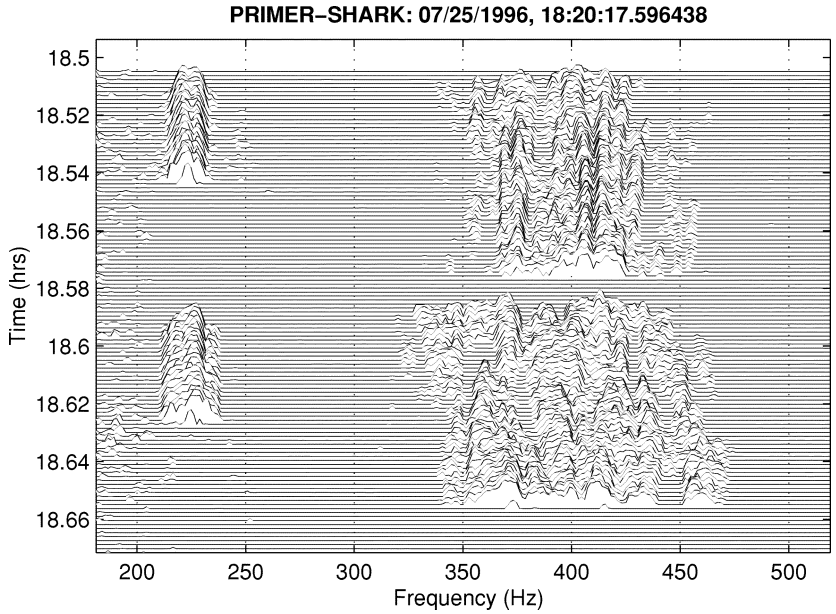

Fig. 6. Uncorrelated 224- and 400-Hz acoustics signal receptions from the PRIMER experiment. Upper 400-Hz arrival is from the SW source, lower from the SE source. The plotting threshold has been set to just suppress out-of-band noise. The minimum value is 0 dB and the maximum value is 25 dB.

layer plays an important role acoustically. Specifically, the warm saline water creates an upward-refracting sound speed profile near the sea floor. This creates an "acoustic shield" for the bottom, reducing the effective bottom interaction.

C. Shelf-Water Meander

The shelf water at the PRIMER site, often called the "cold pool" water, is generally seen as a relatively homogeneous body of cold water extending from 25–90 m in depth. During the summer, this shelf water is commonly found over the continental slope. The frontal boundary is unstable and is frequently contorted due to meandering at wavelengths of 20–40 km. During the SeaSoar observations, a meander with a wavelength of 40 km and a peak-to-trough amplitude of 30 km passed through [11]. The westward propagation of the meander is evident on the map of temperature at 30 m (Fig. 3). On Day 3 (July 28, 1996), the western edge of the meander has pushed the shelfbreak front well south of the southeast acoustic source mooring. The entire acoustic-propagation path from SE to NE is then within the relatively homogeneous cold water of the meander. By Day 5 (July 30, 1996), the cold water is centered in the experiment domain and by Day 7 (Aug. 1, 1996) the front is again north of the southeast acoustic source. The meander can be seen to be as deep as 90 m.

The presence of the frontal meander can affect other aspects of the local oceanography. For instance, the amplitude of the internal tide soliton field, as shown in a subsequent section, appears stronger on the western side of the experimental area, where there is more density stratification. (The homogeneous cold-pool water is less density stratified.) As the meander moves east to west, the stratified thermocline is squeezed into the upper 10–20 m, which has been conjectured by Colosi [12] to partially suppress soliton generation and also to alter the propagation characteristics of these waves.

D. IW Field

IWs are a ubiquitous feature near the shelfbreak, just as they are over much of the continental shelf and in the deep ocean. While the spectrum of the deep ocean IW field is well described by the Garrett–Munk (GM) model [13], an equivalent universal spectrum does not presently exist for shallow water. The shallow-water IW field can be highly anisotropic and inhomogeneous and may contain substantial energy in the form of nonlinear IWs. Analysis of the summer PRIMER data suggests that the nonlinear IW field dominates the linear waves in energy. From an acoustics standpoint, the nonlinear solitary waves, with their larger amplitudes and shorter spatial wavelengths, will also have the greatest effect on propagation; observations of the solitary wave field (also called the "solibore internal tide," as it combines both an internal tidal bore and the high-frequency solitons) will be the focus this section. (We show a detailed rationale of how the nonlinear waves dominate over linear waves in their acoustic effects in the PRIMER region in Appendix A.)

Observations of the soliton field during the experiment were made by numerous thermistors and a near-bottom upward-looking ADCP. While the western side of the experiment site was well-sampled, the eastern side was monitored only by T-pods on the SE and NE acoustic moorings. (This was done purposely to avoid a shipping lane through the eastern portion of our site.) The SE mooring T-pod data showed little vertical structure consistent with traveling solitons or solibores. This could be an indication that the nonlinear IWs were not yet developed at that location and that, perhaps, the wave-generation site was inshore of the SE mooring.The NE mooring thermistor data show some well-developed nonlinear IWs, which we will look at next.

The IWs are most simply described by vertical displacements of the isopycnal (constant density) surfaces in the water column,

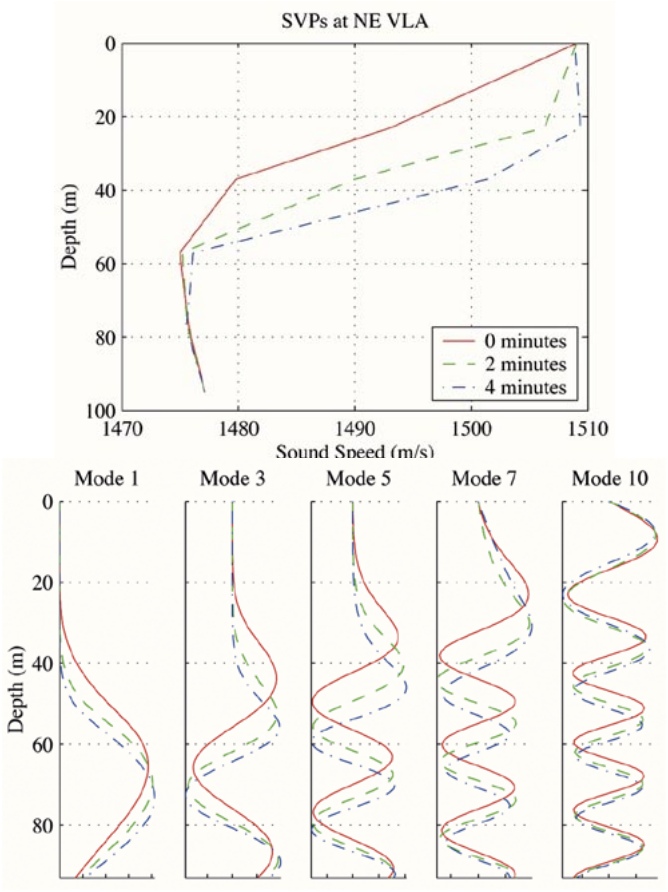

Fig. 7. SVPs and their corresponding mode shapes at 2-min intervals, illustrating the impact of a passing soliton.

so we should examine the density displacement $\eta(x,t)$. Thermistors, of course, provide only temperature and the SeaSoar provided only infrequent (and not colocated) salinity data. This is formally inadequate, as one needs both the temperature and salinity fields to obtain density. One way to solve this difficulty is to employ the isotherm displacements as proxies for density displacement. This uses the relationship $\eta = \Delta T/(\partial T/\partial z)$, which has been shown, in many cases, to be in reasonable agreement with the results from using actual isopycnal surfaces [14].

Fig. 4 shows the 12 °C isotherm as extracted from the NE VLA thermistor pod data. The time series has been broken into consecutive 2×12.42-h segments, which are aligned in the plot. Vertical lines are drawn at 12.42-h intervals to aid in identifying soliton packet arrivals that may be linked to the semidiurnal tide. Since the tide is mixed, however, the semidiurnal dependence is not exact. Moreover, several rank-ordered soliton packet arrivals are apparent, some of which differ substantially from the semidiurnal times. The presence of an underlying solibore depression is apparent in a few of these cases.

Given the apparent randomness of some of the IW arrivals in time, it is likely that solitons are arriving at the NE VLA from multiple generation sites and, moreover, that these sites do not consistently generate solibore/soliton packets. Interestingly, the periods during which the SeaSoar data show the cold-water meander situated over the eastern edge of the region [yearday (YD) 211–213] correspond to periods of reduced soliton activity. In a careful study of packet arrivals at moorings on the western side of the PRIMER area, it was noted that the arrivals had a root mean square (RMS) wander about the 12.42-h period of about 2.4 h [12]. The tidal packets seen at the NE VLA and identified as being most-likely M2 related, show a similar wander in arrival times. Fig. 5 shows the highpass-filtered RMS isotherm displacement at the NE VLA over the course of the experiment. Semi-diurnal fluctuations are clearly visible on several of the days, but are either partially or completely suppressed on others. Thus, we see that the IWs show considerable variability, both in phase (arrival time) and amplitude.

III. Acoustics Measurements

Concurrent with the physical oceanography data, collection was an acoustic-propagation experiment designed to measure upslope propagation through a shelfbreak front and other important oceanography. Vertical receiver arrays were deployed to provide spatial discrimination between the various acoustic normal mode arrivals and m-sequence transmissions were used to provide maximum-pulse arrival-time resolution. This paper considers only the NE array data. The acoustics component of the experiment specifically consisted of four moored tomography sources along the southern edge (three 400 Hz and one 224 Hz) and two vertical receiving arrays at the two northern corners. The transmission scheme called for each 400-Hz source to transmit every 15 min, with each source offset by 5 min to eliminate transmission overlap. The 224-Hz source was programmed to transmit every 5 min. Unfortunately, the 400-Hz source located in the center failed to operate for the entire experiment. In addition to the acoustic source moorings, a series of SUS charges were air deployed on two different days. Geoacoustic inversions from these SUS data [15] provided the bottom geoacoustic model used in the propagation modeling described in Section IV.

A. General Look at Acoustic Observations

Fig. 6 shows an example of unprocessed individual m-sequence arrivals at the NE VLA from the three operating sources. The 224-Hz source pulse arrives every 5 min and the SE 400-Hz (upper) and SW-400 Hz (lower) pulses arrive every 15 min, with 5-min offsets between sources. The peak-to-noise floor spectrum level is 25 dB, where the plotting threshold has been set to just suppress the out-of-band noise. As would be expected, the SW 400-Hz arrival, which has to travel over a longer path, shows more attenuation than the SE 400-Hz signal. This is best evidenced by the lower signal levels toward the upper edge of the frequency band. The 400-Hz receptions also contain numerous nulls, or notches, in the spectra, which are stable over time scales of 2–3 min. Similar instances of frequency-selective fading are seen in virtually all of the transmissions from both sources. These are due to broad-band multipath interference effects.

The vertical array that we employed both for gain and acoustic normal mode resolution was a 14-element array spanning the lower 53 m of the 90-m-deep water column at its location. Array motion was monitored using travel times from three high-frequency transponders surrounding the array. Four

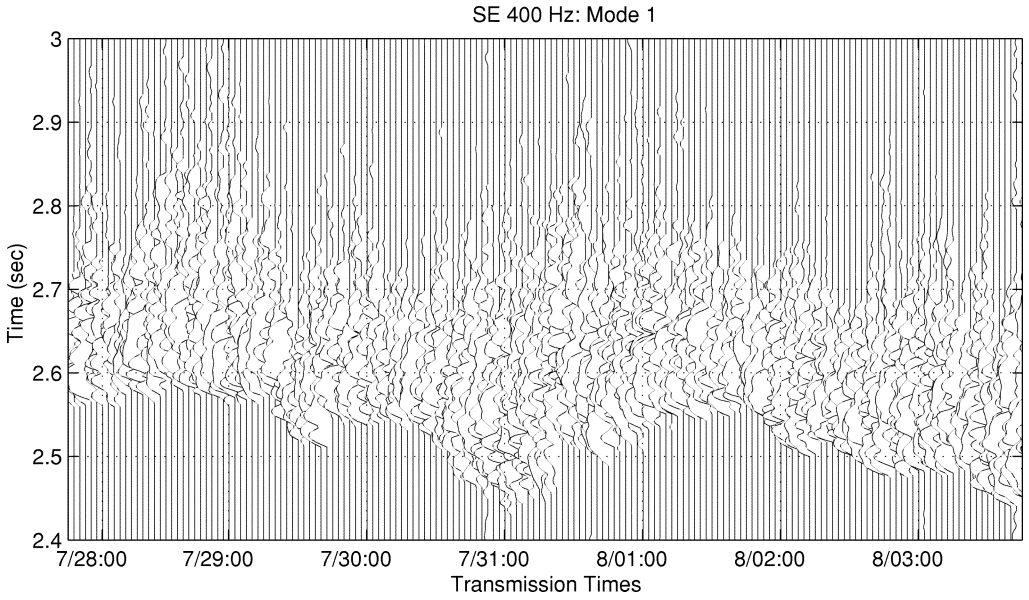

Fig. 8. Waterfall plot of mode-1 pulse arrivals from the southeastern source, illustrating both the spread and the wander of the mode pulses. The minimum level is 0 dB and the maximum level is 35 dB.

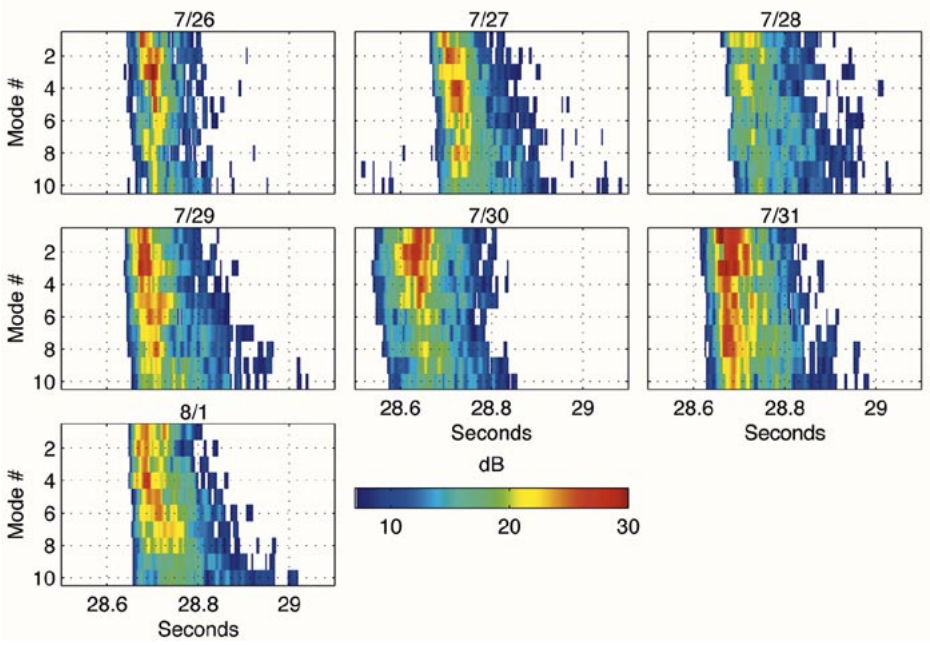

Fig. 9. Mode-arrival energy for the first 10 modes from the SE400-Hz source, averaged over a 1-h period during the middle of each SeaSoar transect along the eastern edge.

hydrophone channels were configured to receive and process the transponder signals. Estimates of array motion showed little movement, in accordance with the fact that the mooring was quite stiff and the upper float was well below the strong surface currents. Because the array spanned only the lower half of the water column, discrimination between the normal modes was less than ideal, but certainly sufficient to provide very good resolution of the first two or three modes. For higher modes, there was filtration leakage into neighboring modes, so that one is generally looking at the average of two to three closest neighbor modes. The thermistors on the VLA itself proved invaluable in calculating the local mode shapes for mode filtering (Fig. 7), as the temperature structure fluctuated significantly and on quite rapid time scales. Fewer thermistors or longer sample periods would have seriously aliased our monitoring of the fluctuations and degraded the modal decomposition.

The waterfall plots in Fig. 8 show the amplitude of the mode-1 arrival from the southeastern 400-Hz source (abbreviated as SE400). Each transmission lasts roughly 4 min (1 transmission $= 48$ m-sequences, each of 5.11 seconds' duration). Within an individual 4-min transmission, the receptions are reasonably correlated; however, across transmissions, the correlation is weak. The maximum decorrelation time, therefore, is at most 11 min, but is likely much less than that. (In a few instances there are features that are consistent from one 15-min period to the next, but not generally.) The mode-1 arrivals also

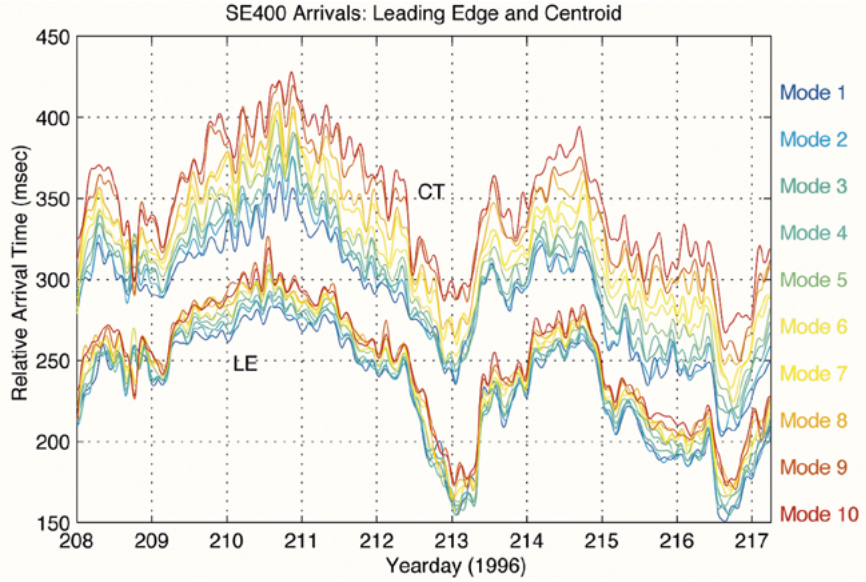

Fig. 10. Leading edges (LE) and centroids (CT) of normal mode arrivals from the SE400-Hz source.

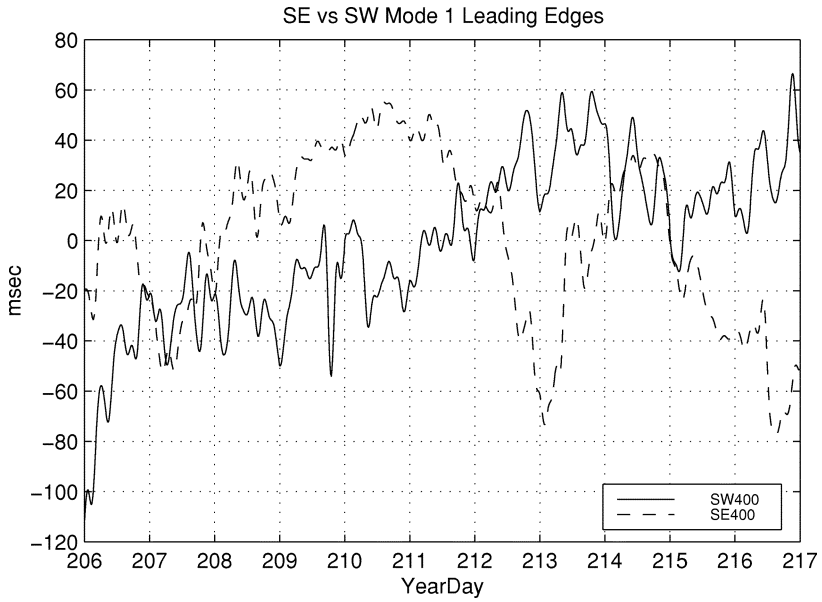

Fig. 11. Leading-edge arrivals of mode 1 from the SE and SW 400-Hz sources, showing the disparity between the two paths.

show a time spread that is far greater than that imposed on a 10-ms pulse by normal waveguide dispersion. In fact, the spreads are generally of order $R/(v^G_{n\,\text{slowest}} - v^G_{n\,\text{fastest}})$, which implies that the mode-1 final state observed came from the entire spectrum of trapped modes, which coupled along the path.

Fig. 9 shows the output of the modal beamformer for the SE400-Hz source receptions over a seven-day period. Each panel represents the modal energies averaged over a 1-h period each day, during which there was SeaSoar sampling along the eastern leg. There are many interesting features to note. First, there is a daily wander in all of the mode arrivals of over 100 ms; the relative arrival times of the individual modes varies substantially on a daily basis as well. The energy distribution among the modes is also quite variable from day to day. There is, additionally, a roughly 200-ms time spread to the arrivals, although, on some days (July 27 in particular), it is less than 100-ms for the lower modes. In Section V, we will use propagation-modeling tools based on the environmental data discussed in the previous section to develop an understanding of why the arrivals shown in Fig. 9 look the way they do.

B. Modal Statistics Definitions

In the following section, we will describe the fluctuations of the modal arrival times in terms of the first and second moments. Such measures are useful for both correlation with the PRIMER physical oceanographic variability and for providing predictions of arrival behaviors in similar regions. We note that the terms "pulse wander" and "pulse spread" are often used in describing these moments and will be adopted here.

Several different parameters were considered as measures of the signal wander, including the leading edge of the arrival, the arrival centroid, and the peak amplitude arrival time. The leading edge of the arrival was defined to be the first time the

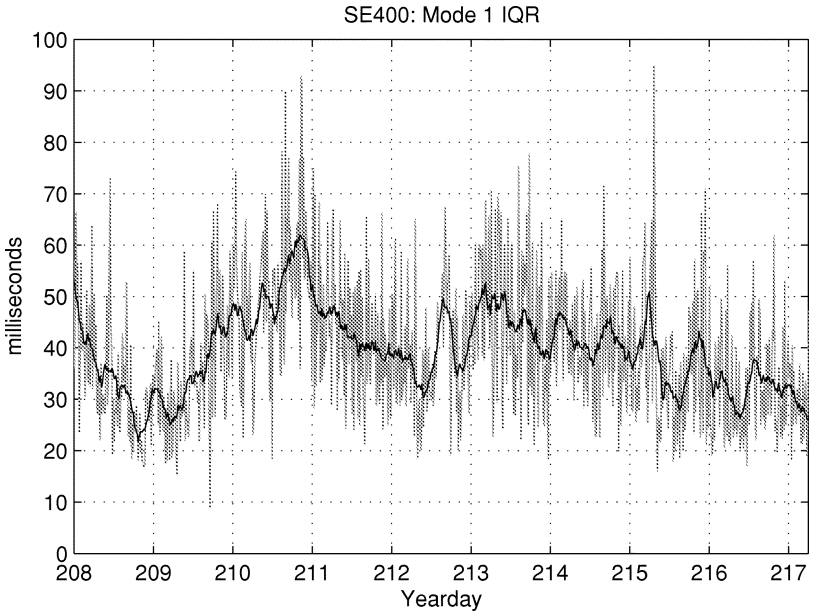

Fig. 12. IQR spread of the 400-Hz mode-1 arrival, with raw numbers in gray and lowpassed version in black.

arrival transitioned through a threshold set to 15 dB above the noise floor. The noise floor was determined for each transmission by calculating the background noise level based on a short section of data prior to any arrival. Arrivals that were obviously contaminated by shipping noise were eliminated from consideration. The peak arrival time was defined simply as the time of arrival of the point of maximum amplitude in the time series. The centroid was calculated by finding the center of mass for that portion of the sequence that was above threshold.

There are a number of ways one can define the spread of an arrival, such as variance, time above threshold, interquartile range (IQR), mean absolute deviation, etc. Due to its success in similar situations [16] and because a survey of other measures failed to uncover a better statistic, the IQR is used here as a measure of signal spread. The IQR is defined as the difference between the 75th and 25th percentiles and is a robust estimator of the spread.

The leading edge and other statistics were computed for each of the 48-m sequences in a full transmission and then averaged together, creating a time series of mode statistics with a 15-min sample period. (Recall that the 400-Hz sources each transmitted a string of 48-m sequences, lasting a total of 4.1 min, every 15 min.) Initially, these time series are given a 4-h running average to remove the high (oceanographic) frequency fluctuations, which are themselves of interest and are analyzed later on. Another measure of interest is the variance of the various statistical measures available. In particular, the variance across the 48-m sequences that were used to create each 15-min sample point is useful to know. In the sections that follow, we look at the wander and spread of the source receptions. Where appropriate and possible, comparisons are made between the acoustic data and the oceanography.

C. Pulse Wander

In this section, we look at the travel-time wander of acoustic arrivals due to various oceanographic effects. In particular, we examine the effects of mesoscale-to-large scale oceanography and tidal frequency phenomena, including the east–west geographical differences at the PRIMER site. We begin by looking at the mesoscale and larger scale oceanography effects.

Fig. 10 shows the leading edges and centroids for the first ten acoustic normal modes. Several correlations may be drawn between the acoustic variability and the large-scale oceanography picture provided by the SeaSoar data. For example, the period between YD 209 and 212 contains the cold-shelf-water intrusion along the eastern propagation path, as the frontal meander passed through the study area. This is reflected by the generally longer travel times of all the acoustic modes. The sharp decrease in travel time centered around the beginning of YD 213 (July 31) coincides with the movement of the shelfbreak front north of the SE source. Over this span of 72 h, the mode-1 leading edge undergoes a travel-time change of over 120 ms. If this were to come entirely from a change in average water temperature along the acoustic travel path, it would require a ΔT of 1.3 °C, assuming an average mode-1 group velocity of 1480 m/s. This is found to be in good agreement with the findings from a simplified acoustic inversion for range- and depth-averaged water temperature [17] that is compared to both SeaSoar and thermistor records.

Next, we look at the east–west geographical differences in the larger-scale oceanography and its acoustical effects. Fig. 11 shows the leading edges of the mode-1 arrival from the SE and SW 400-Hz sources. The pulse travel-time series from the two sources appear rather different and, in some places, they appear to have opposite trends. The SW400 path undergoes a total change of 170 ms, as compared with 130 ms for the SE400 path. Based on analysis of the SeaSoar data covering YD 208–214, the increase in travel time seen first in the eastern path around YD 208 and later in the diagonal path around YD 211 is consistent with the shelf-water meander being pushed to the west, creating slower travel times along the occupied propagation paths.

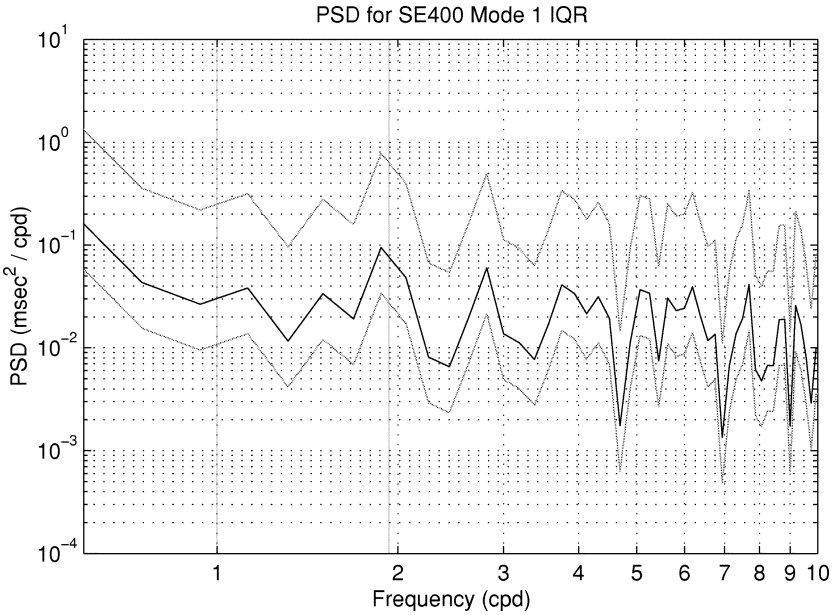

Fig. 13. Power spectral density estimates for the SE400 mode 1 IQR. Gray lines indicate the 95% confidence limits.

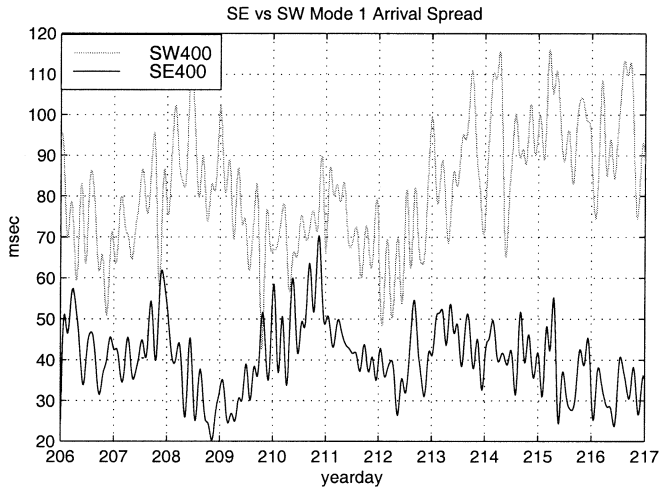

Fig. 14. Mode-1 IQR arrival spreads from the SE and SW sources. The difference in overall average arrival time is due to path length. The difference in shape is due to the traversal of different oceanography by the two paths.

On YD 213, the SW400 path reaches its slowest travel time, which matches very well with the SeaSoar data that shows the meander encompassing the entire SW400 propagation path at that point. The same travel-time value is reached again just before YD 217, perhaps indicated that a similar environment has been reached. Thus, we see that the large-scale oceanographic variability and the acoustic travel-time fluctuations are consistent, both along the eastern track and across the tomography array.

We next turn to the tides. It is well known that a certain amount of travel-time variability will result from tidal activity on the continental shelf. For instance, calculations by Headrick *et al.* and Sperry [5], [17], among others, have shown how tidally driven solibores can introduce tidal period wander and mode coupling: however, there are also many other direct means by which the tides can influence the acoustics. These include tidal currents (both barotropic and baroclinic), horizontal advection of water masses by the tides, and the simple barotropic change in water depth.

Interestingly, while tidal-period effects on acoustics are always substantial for the NW receiver in PRIMER (Chiu, private communication), they are often smaller for the NE receiver. The previous figure, showing the leading edge and centroid arrivals for the eastern (SE to NE) propagation path, shows only slight arrival-time variability at tidal frequencies. This is supported by a power-spectral-density analysis of the mode-1 pulse-arrival leading edge (not shown here). So, while there may indeed be contributions at the diurnal and semidiurnal frequencies, they do not stand out significantly from the rest of the spectrum for our NE VLA receptions. Nevertheless, as an item of general usefulness, we are still interested in estimating the contributions to travel-time variability from various tidal components, and will do so next.

Tidal current effects, both barotropic and baroclinic, tend to be small (of order vR/c^2), where v is the current magnitude, R is the source–receiver separation, and c is the average sound speed of the water column. If we use reasonable numbers for our case, i.e., $R = 42$ km, $c = 1500$ m/s, and $v = 10$ cm/s, we get travel-time wanders on the order of 2 ms. Generally, the observed amount will be even less, in that we have assumed here that the current is constant along the 42-km path, which it probably is not.

The effects of horizontal sound speed structure advection by the tides are generally difficult to estimate, but we will proffer one example. The north–south tidal-excursion lengths (obtained by integrating the tidal currents generated by a data-based tide model) are ± 1000 m. If, at its maximum southern displacement, the northern edge of the front was just seaward of the source, the changing tide could advect the front a full 2 km northward of the source. Assuming an average change in water temperature of $1\,^{\circ}$, this influx of warmer water could result in a 4-ms decrease in travel time.

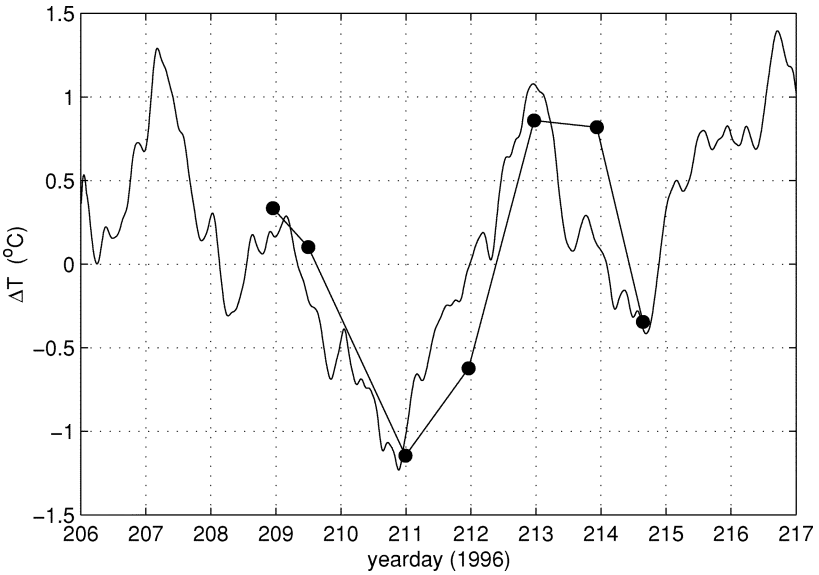

Fig. 15. Average change in average temperature along the SE400-Hz source path versus direct measurements of that quantity from SeaSoar data.

Water-depth changes are available from the same tide model that provided the barotropic current field. The maximum variation appears to be ± 80 cm. The acoustic impact of such elevation changes was estimated by assuming adiabatic propagation over the 42-km path length. For the lowest five modes, there is virtually no change in travel time, owing to their very weak interaction with the surface waters. For surface-interacting modes, there can be changes of 10 ms or greater. The two simplifications that were made here—spatial uniformity of the tidal elevation change and adiabatic propagation—suggest that these numbers should be treated as extrema; specifically, they are an upper bound on the higher-order modes and a lower bound on the lower-order modes.

Turning to the regional variation of the tides, of first-order interest is the enhanced M2 signal seen in the acoustics on the diagonal path from the SW source to the NE receiver. There is, seemingly, a simple explanation for this, which is that the M2 internal tide is simply more energetic on the western side of the site, as measured by thermistor data [12].

D. Pulse-Time Spreading (Variance)

We next look at the time spreading of acoustic arrivals due to various oceanographic effects. We will concentrate here on tidal-frequency phenomena and the east–west geographical differences at the PRIMER site. We also will look at the phenomenon of the "near receiver dominance" of the spreading that was described by Headrick *et al.* [5], [6] during the SWARM experiment. We concentrate on M2 internal tidal effects, with an emphasis on the scattering by solitons.

Fig. 12 shows the signal spread, as measured by the IQR, for mode 1 for the SE source receptions. Higher modes were seen to have progressively more spread (not shown here), some of which is due to increasing amounts of modal filtration leakage ("crosstalk") from the aperture-limited mode filtering [17]. The values shown in Fig. 12 are very comparable to the spread seen in the SWARM data [5], except that a factor of two more daily variability is seen in the PRIMER data. The increased daily variability is perhaps not unexpected, given the proximity to the highly range-variable shelfbreak front oceanography, which is advected by the tides, as well as the longer path lengths. The

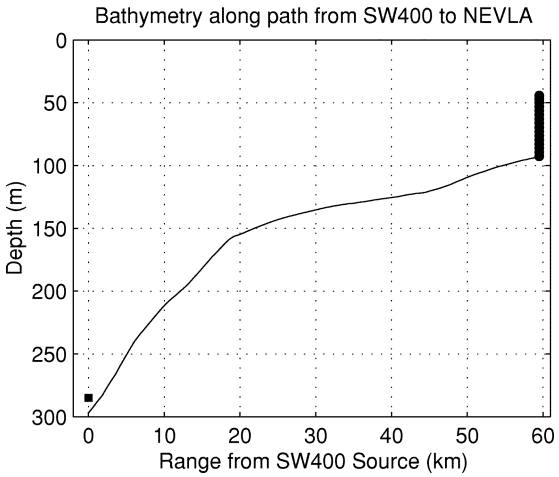

(a)

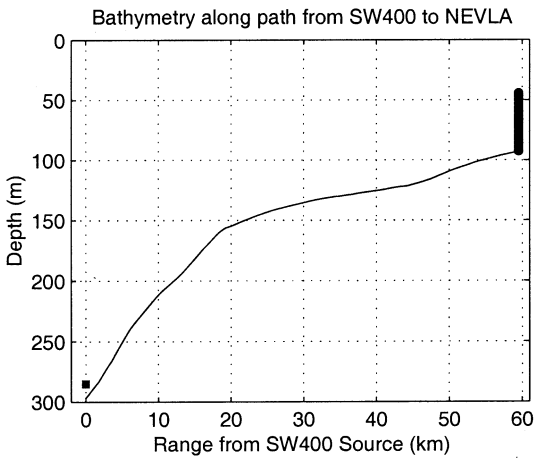

(b)

Fig. 16. (a) Bathymetry for the eastern edge, across the shelf-propagation path. (b) Bathymetry for the diagonal path from the SW source to the NE VLA.

decreases in time spread during yeardays 209 and 212 correspond to periods that appear to have less soliton activity, as inferred from the relative quiescence of the thermistor data at the NE VLA. This observation is further quantified by highpass filtering the RMS isotherm displacement at the NE VLA, as shown in Fig. 5. The decrease in spread centered around YD 212-213 corresponds to a minimum in soliton activity near the NE VLA. However, the large decrease in the spread of mode 1 around YD 209 (July 27) does not correspond to a similar decrease in soliton energy at the NE VLA, so that the amount of near receiver energy in the soliton field obviously does not tell the whole story. Fig. 13 shows the power spectral density of the IQR shown in the previous figure. Note the large peak at around two cycles per day, indicative of M2. The dominant contribution to this peak is likely mode coupling from solitons that have been generated at the M2 tidal cycles, as the coupling due to solitons is strong and solitons are numerous along the acoustic paths.

We next look at the east–west dependence of the time spreading. Fig. 14 shows both the SE400 and SW400 signal spreads for mode–1 arrivals over several days. Readily apparent is the fact that SW400 arrivals experience much greater spread than those along the eastern edge. A small amount of the difference in spread can be attributed to increased effects of frequency dispersion due to the longer propagation path. A longer path also represents more opportunities for mode coupling to occur. Moreover, the stronger IW field to the west would certainly contribute to more coupling and spread. In addition to having higher levels of spread overall, the SW400 arrival spread also shows greater variance, which again may be attributed to the longer path length.

E. The Shallow-Water Tomographic Inverse Problem

One of the original goals of the PRIMER experiment was to use the acoustic data to invert for the temperature field throughout the region. This proved to be rather difficult, in large part because of the large amount of mode coupling, which we have discussed. In lieu of a full coupled mode inverse, as is being pursued by Chiu (C. S.Chiu, private communication), we attempted to see how well we could do just using the single "mode-1 leading edge" data point that was readily available. In this section, we show the result of those (adiabatic mode) calculations.

In Fig. 15, the small dots represent range- and depth-averaged temperatures computed directly from SeaSoar records. There is reasonable agreement between the acoustic temperature estimates and the SeaSoar results, but they do not follow exactly. Near days 212 and 214, the results are off by half a degree or more. There are numerous factors that probably contribute to the discrepancies but, again, the most likely is mode coupling. By not taking into account the actual path through the mode space that resulted in each $\tau_n(t)$ data point, one is almost assured of not achieving the correct answer. Some speculation regarding the large discrepancy near Day 214 is in order. That is the day where there is the largest intrusion of the shelfbreak front northward of the SE400-Hz acoustic source. The SeaSoar data indicate much more of a warming than the acoustic data show, relative to the seven-day mean. Recall that there was enhanced coupling into the lower modes near the front during YD 213. Also recall that over the first half of the propagation path, the lower modes are traveling the slowest. Therefore, in spite of there being more warm water near the source, much of the received acoustic energy is actually arriving later than usual because it has to travel in lower modes early on in the propagation path. If one assumes that the increase in average temperature around YD 213 is due to the front being advected north of the source, then one might surmise that similar events are happening shortly after YD 207 and a little before YD 217. This is consistent with observations from the thermistors on the southeastern source mooring.

IV. Propagation Modeling

One of the most valuable aspects of the PRIMER experiments was the high temporal and spatial resolution of the physical oceanography data that was taken concurrently with the acoustic data. This section presents the results of a detailed propagation study that incorporates the oceanographic data into a wide-angle parabolic-equation (PE) propagation model [18]. The PE model is the method of choice here because of its numerical efficiency in handling the strong range variability found near the shelfbreak. However, while PE efficiently provides the complex pressure field, it does not give the direct physical insight that the ray- or mode-propagation pictures provide. To aid in understanding the underlying propagation physics, the PE field is thus projected onto the local mode shapes, as computed by a standard normal mode code [19] at numerous ranges and frequencies. By following the transfer of energy between modes and also the variations in mode-group velocities, a picture may be formed of how the oceanography affects acoustic propagation. The propagation modeling task has been broken down into three levels of complexity. The first is the reference, or mean, environment, which includes the bathymetry and only an average representation of the sound velocity field, neglecting any temporal mesoscale or finer variability. This reference environment would correspond to the first-order environment that might be used in a perturbation analysis. The second level of propagation modeling adds in the spatial and temporal variability of the mesoscale field. This is provided by the SeaSoar data. The third and final level is the fine-scale variability provided by the thermistor records. The primary component here is the IW field.

A. Bathymetry and Geoacoustics

Fig. 16 shows bathymetric sections along the eastern and diagonal propagation paths to the northeast VLA. The data were taken from the National Ocean Survey (NOS) Digital Bathymetric Soundings, as distributed by the National Geophysical Data Center (NGDC). Comparisons of the data with shipboard echosounder data indicated that the two datasets are in good agreement, with variations on the order of 2–3 m. The initial upslope portion of both propagation paths is relatively steep, reaching a maximum slope of 2.5 $^\circ$ on the eastern path. It is considerably less steep on the continental shelf.

With a representative sound speed model for the water column established, as well as the bathymetry, the remaining ingredient necessary for acoustic-propagation and scattering calculations is the sea-bottom geoacoustic properties. A typical

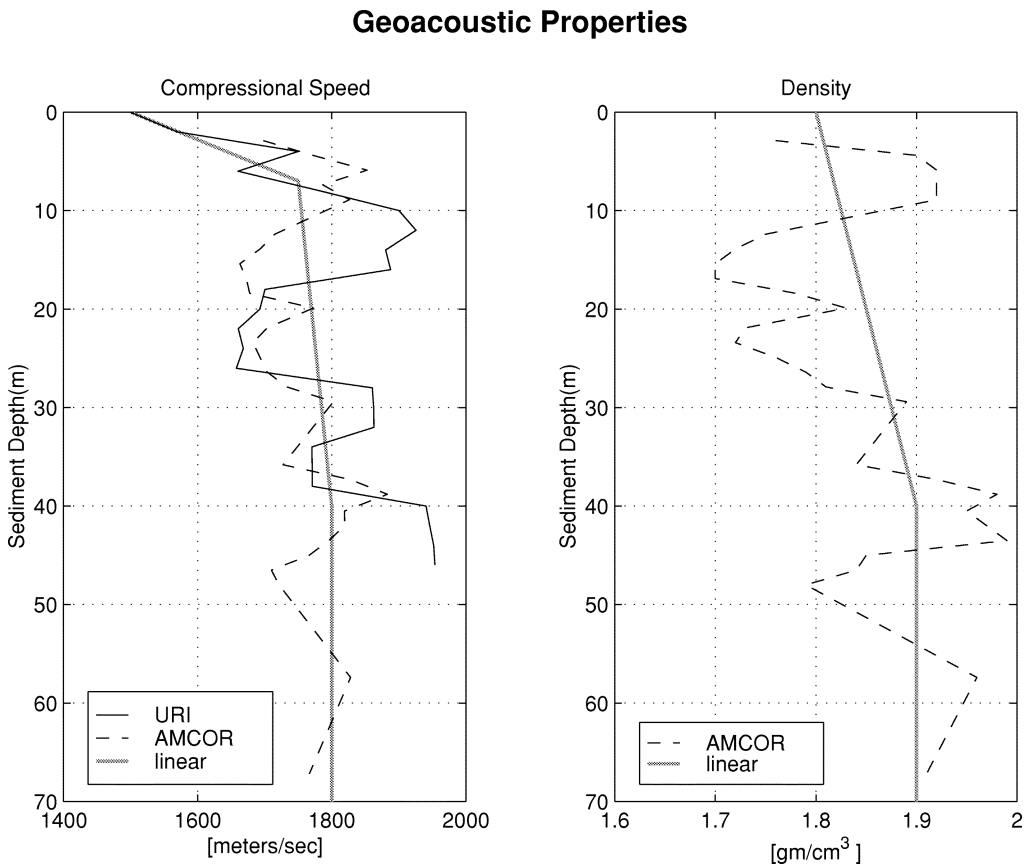

Fig. 17. Geoacoustic properties of the fluid bottom (compressional wave speed and density) for the PRIMER experimental site, based on SUS shot measurements (denoted URI) and core measurements (denoted AMCOR).

sediment profile in the region of the PRIMER experiment consists of an upper layer of Holocene sands, 5–20 m deep, followed by up to 200 m of horizontally stratified layers containing various mixes of silt, sand, and clay material from the Pleistocene era [15]. The sandy surface layer may also be composed of medium-to-coarse-grained sands or even gravel in some locations. While the continental shelf areas surrounding the PRIMER site have been well studied, there is virtually no published geoacoustic data available for the upper 100 m within the actual study region. An Atlantic Margin Coring (AMCOR) project drill site was located about 20 km due west of the southwestern corner of the experiment, which provides core data down to about 300 m [20]. Another source of geotechnical data is from the SUS-based geoacoustic inversions that were performed as part of the PRIMER experiment itself, along with several shallow cores that were done post-experiment [15]. Profiles of compressional velocity and density are shown in Fig. 17, for both the AMCOR core and recent geoacoustic inversion results obtained from the SUS by the University of Rhode Island (URI) group. Since no direct measurements of compressional wave attenuation were available at our frequencies, standard values were used for the propagation modeling.

B. Upslope Propagation, Bottom Effects

It is necessary to first establish a time-independent reference-propagation environment before addressing the acoustic effects of the time-varying regional oceanography. To accomplish this task, the mean cross-shelf stratification is obtained by averaging the SeaSoar records both in the along-shelf direction and temporally, thereby collapsing a four-dimensional (4-D) environment into a two-dimensional (2-D) slice. Fig. 18 shows an average SVP for the eastern section, computed by temporally averaging the appropriate SeaSoar sections. It is interesting to note that, despite the sometimes dramatic differences in profiles between the few days data we have, the mean field bears a striking similarity to that found by Linder and Gawarkiewicz [9] in a study of climatology of the area.

During the summer PRIMER experiment, each of the 400-Hz sources was moored just 12 ms above the bottom. In looking at Fig. 18, it is clear that a deep source is not the most efficient way of getting sound into the shelf waters; a source located mid-water, within the shallower cold-water duct, would have been optimal. However, for the PRIMER experiments, engineering practicalities dictated that the source be placed very near the bottom. In particular, such placement substantially reduces mooring motion.

To understand how the sound field generated by the PRIMER near-bottom sources is affected by upslope propagation, PE simulations were made using the environment described earlier and the computed pressure field projected onto the local mode shapes at each range step using standard techniques [21]. Fig. 19 shows how the mode amplitudes vary as a function of range and mode number. (Cylindrical spreading loss is *not* included in these simulations, since it is uniform with mode number.) Looking first at the initial mode amplitudes at the source, the

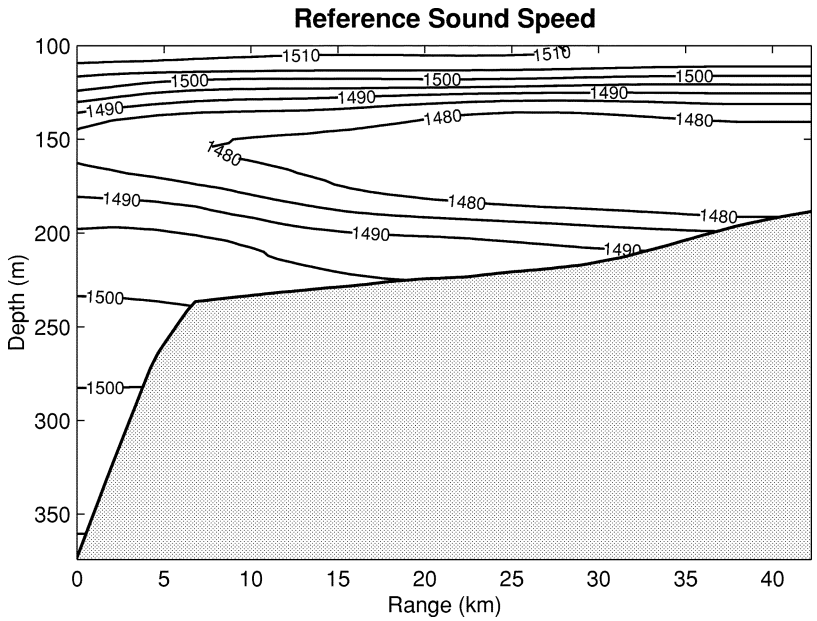

Fig. 18. Average "reference" sound speed for across-shelf propagation at the PRIMER site.

pattern is consistent with that of a near-bottom source exciting only the higher modes that have nonzero amplitudes near the bottom. The source depth passes through zero-crossings of the mode shapes as mode number increases, giving rise to the null at around mode 21. The anomalously large amplitudes in modes 5, 7, and 9 are because those particular mode numbers correspond to modes that are trapped in the narrow duct just above the ocean bottom. These bottom-ducted modes die out within a few kilometers of the source due to both attenuation and because they couple well into higher modes (10–15) that are not trapped in the lower duct, but do extend all the way to the bottom.

From Fig. 19, it is seen that the primary effect of the bottom slope is to strip out energy from the higher modes. The energy in "middle" modes 10–20 is seen to be able to propagate onshore reasonably well without excessive loss. For most of the shelf-propagation path, modes five and lower are nonbottom interacting. Although much energy is lost into the bottom coming onshore, some of the initial high mode energy also couples into the middle and lower modes, so that it is not entirely lost. At the receiving VLA, there are roughly 20 modes with grazing angles below the critical angle in this simulation. An important conclusion that may be drawn from these calculations is that, given the PRIMER source location near the bottom, it is highly unlikely that bathymetric-induced coupling transferred energy into modes 5 and below, where energy was seen in the PRIMER acoustic data shown in the previous section. Some other mechanism(s) must be responsible for this energy transfer, as will be seen.

Aside from the distribution of energy across mode space, another aspect of the background propagation we might usefully consider is the temporal behavior of the signals. Two questions in particular one might ask are: Which modes are fastest and how much dispersion is there? One factor greatly complicating the propagation is the fact that the sound channel near the source is more representative of a deep-water sound channel,

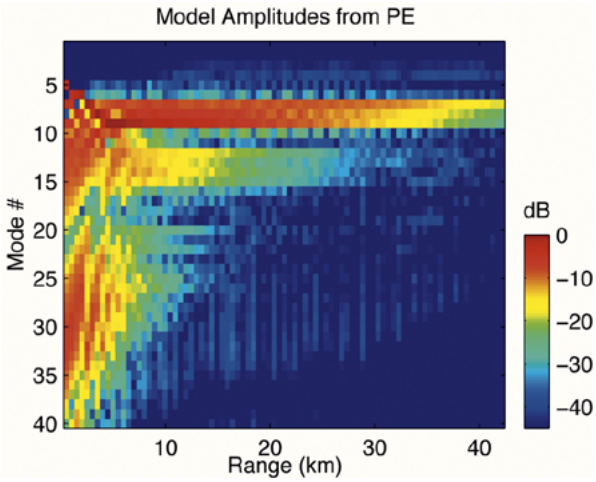

Fig. 19. Modal amplitudes at 400 Hz as a function of range from the acoustic source for the eastern track of the PRIMER experiment. These mode amplitudes are based on local mode projections on an acoustic field generated by the RAM parabolic equation program.

where the higher modes travel faster than the lower modes. Near the receiver, the channel is more typical of shallow-water environments, where mode one is the fastest. Fig. 20 shows the group velocities of the modes as a function of range for the first 20 modes. We see that the fastest path through "mode-number space," going from source to receiver, is in mode 6 until the 30-km mark and then coupling into mode 1 for the remainder.

C. Mesoscale Oceanography Effects

In this section, we will look at the acoustic effects of the daily variability of the mesoscale oceanography over seven days, as measured by the SeaSoar sections. This will be examined in light of several acoustics issues. Specifically, the energy transfer between modes is considered, as are travel time issues. Both PE and adiabatic mode simulations are contrasted to highlight the

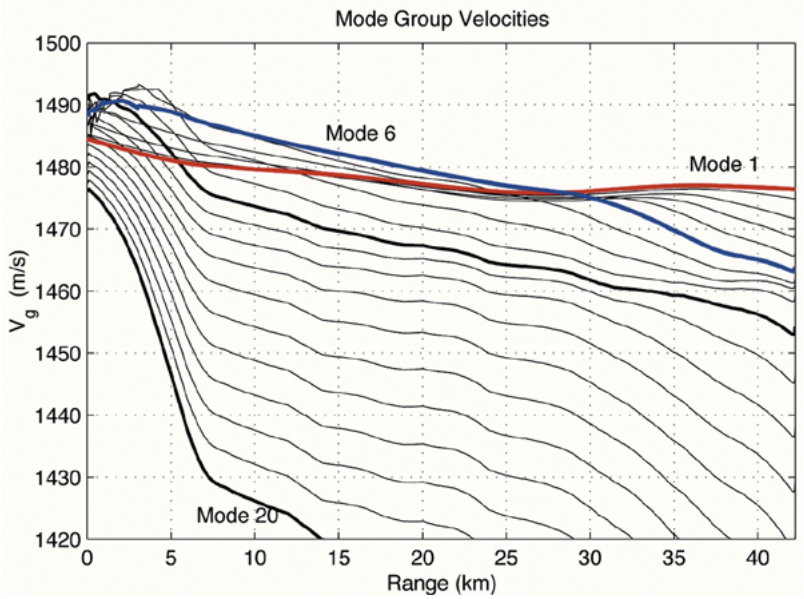

Fig. 20. Modal group velocities for 400 Hz as a function of range for the first 20 normal modes.

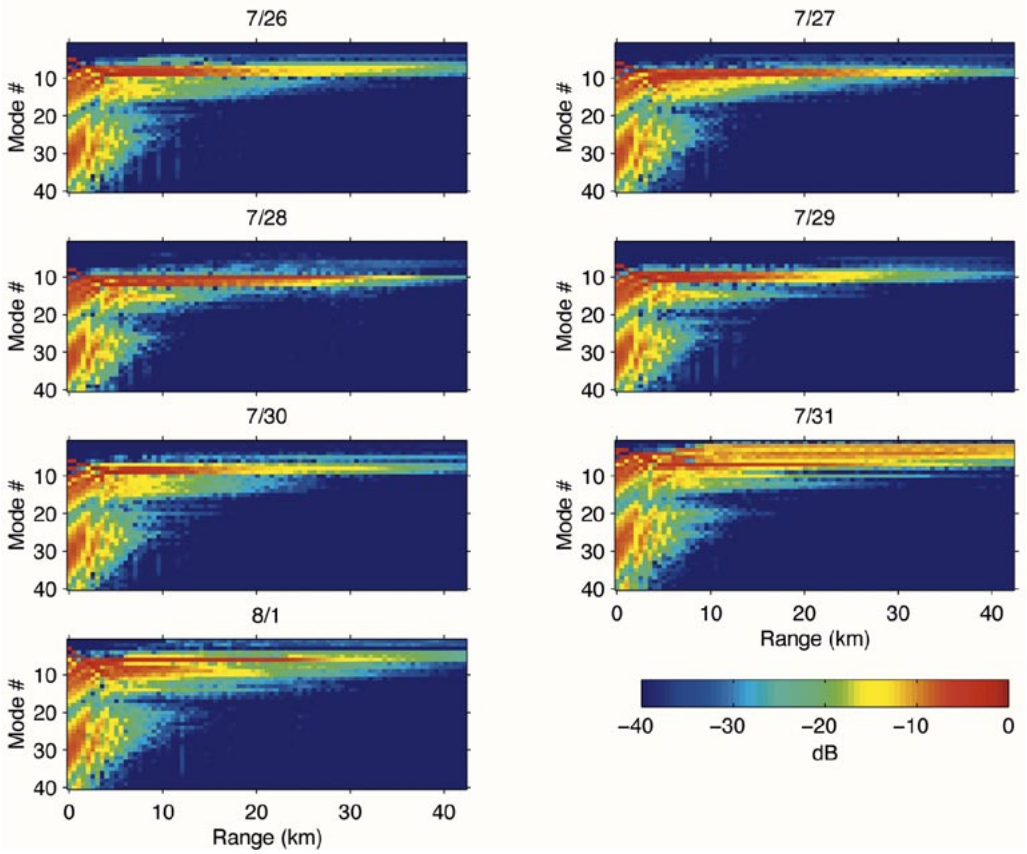

Fig. 21. Evolution of modal energies as a function of range for each of the seven SeaSoar-based sound speed fields along the eastern edge of the PRIMER experiment site.

effects of mode coupling by the front. Finally, we examine some 3-D propagation effects.

We begin by examining the effects of the mesoscale variability on the distribution of modal energy. Fig. 21 shows the mode energies versus range for the seven sound speed sections shown earlier. For July 27 to July 29, when the ocean range dependence is at its weakest, the maximum mode energies are clustered around modes 5–8. For the other days, the energy is spread more evenly among the modes. On July 31, strong low-mode energy is seen at 6 km from the source as a result of the higher modes encountering the large downwelling feature that can be seen in the SeaSoar data on the seaward edge of the front. Thus, one sees that the low acoustic modes can certainly receive energy via coupling due to a strong frontal fea-

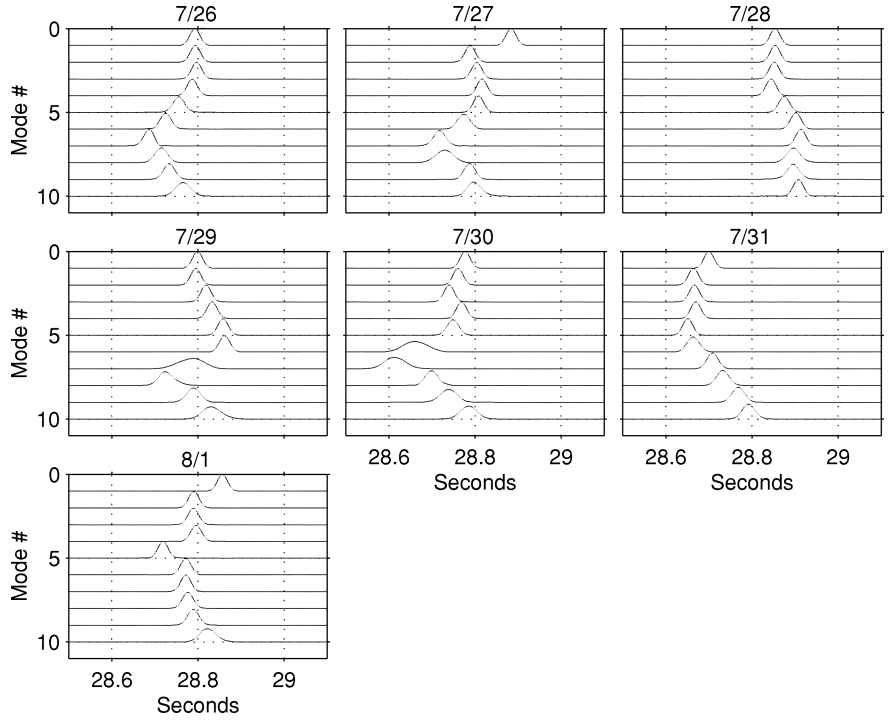

Fig. 22. Mode arrivals from adiabatic propagation through mesoscale variability along the eastern path. All modes were uniformly excited.

ture, but also that this mechanism is intermittent. The front is not able to keep low modes continually present in the acoustic reception data. In fact, in only one of the three days the SeaSoar data actually captured the front was a downwelling cell seen. However, the occurrence of such acoustically significant frontal phenomena is also becoming somewhat more possible to predict, as the downwelling should occur on the flanks of a propagating meander due to local accelerations along the front intensifying the secondary circulation.

We next look at travel-time effects. Measured travel-time fluctuations for a given mode can result from two different effects. The first is due to changes in modal group speed and results from changes in the sound speed field (generally due to temperature) along the propagation path. This is considered here using an adiabatic travel-time change. Mode coupling can also create perceived changes in travel time, but unless these effects can be identified as coming from specific mode-coupling locations, they may be incorrectly ascribed to adiabatic fluctuations. We now look at the magnitudes of these effects.

We consider first the magnitude of the adiabatic travel-time fluctuations. Fig. 22 shows the results of propagating through the seven daily SeaSoar sections, assuming both adiabatic propagation and uniform mode excitation. There is a surprising amount of variability in mode-arrival patterns over the daily sections. The fastest arriving mode ranges between numbers 4–8 and varies by more than 200 ms over the seven days. The spread in mode arrivals also varies substantially, from 50–200 ms. It is apparent that information on the mesoscale structure is being conveyed in the differing mode-arrival patterns. This structure, however, will be modified by the effects of mode coupling and by the fact that the lower mode numbers are not directly excited at the source. All of these effect are considered next, by making broad-band calculations with the PE code, followed by the usual modal decomposition.

Fig. 23 shows the PE-generated (coupled) mode arrivals for the same SeaSoar sections as were displayed earlier. There is significant variability over the seven days. Similar to the adiabatic case, the arrivals wander by up to 200 ms. With mode coupling present, however, the relative arrival structure of the modes is somewhat changed. From July 30 to August 1, more energy in the lower modes is shown than earlier days. This can be traced to mode coupling at the front, which is pushed forward of the SE400 source during this time period.

Another issue to consider is horizontal refraction. It is well known that acoustic propagation at oblique angles to a sloping bottom can result in a deflection, or refraction, of the direction of propagation (see [22]). In terms of normal mode theory, this may be seen by noting that modal phase speeds decrease with a shoaling bottom (provided the sound speed does not drastically change) and that acoustic energy will always refract toward regions of slower sound speed (Snell's Law). To estimate the effects of horizontal refraction for the PRIMER experiment, the "horizontal ray/vertical mode" theory developed by Weinberg and Burridge [23] was applied using the USGS bathymetry for the region and a 3-D sound speed field constructed from SeaSoar data. In the worst case scenario, the differences in mode travel times between straight-line propagation and the horizontally refracted path were less than a millisecond [17]. Straight-line propagation from source to receiver can therefore be assumed, given the smallness of this effect.

D. Small-Scale Oceanography Effects

In addition to the mesoscale oceanography, the small-scale oceanography can also show significant range variability and, thus, induce both adiabatic and coupled mode effects upon the acoustic field. This section looks at what the predicted effects of soliton trains (the high-frequency component of the solibores)

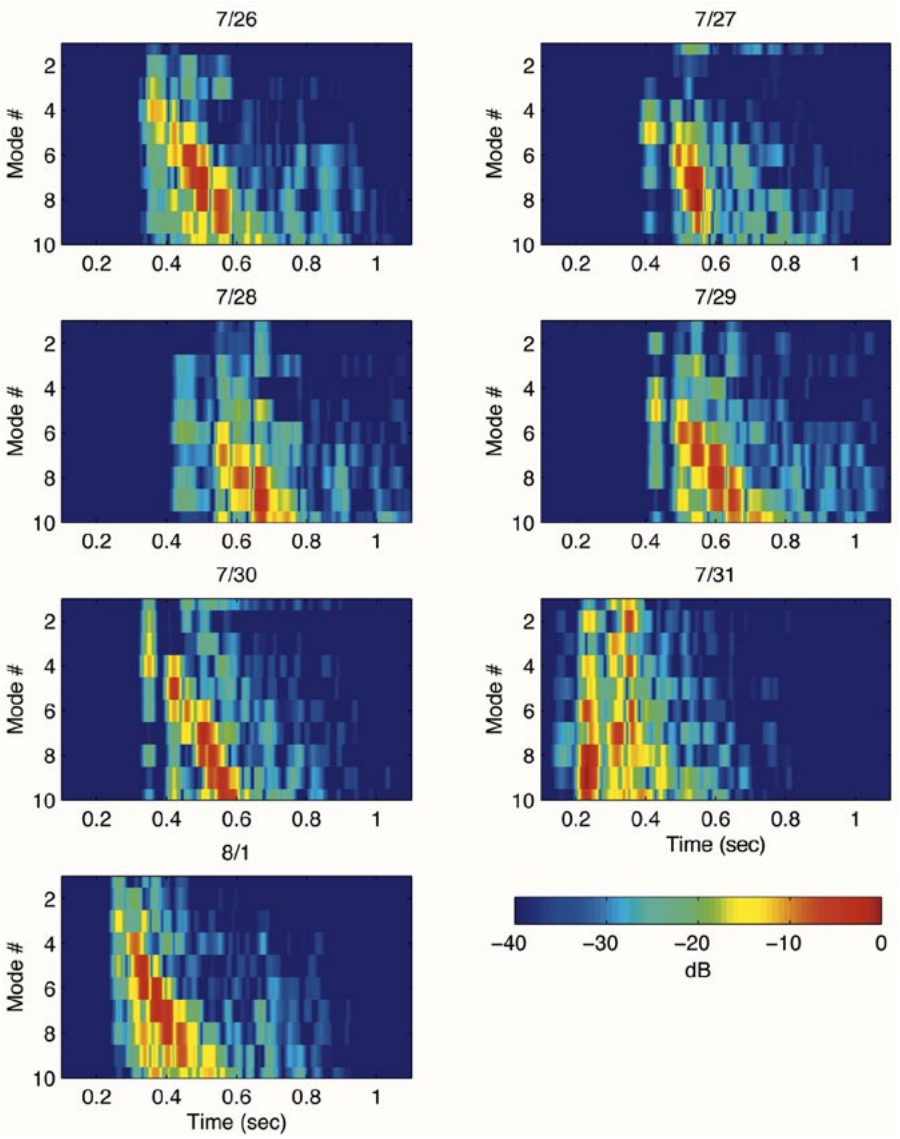

Fig. 23. Synthetic mode arrivals based on SeaSoar sections along the eastern edge.

[24], [25] have on modal propagation and scattering. There also exists a linear IW field and other fine-scale ocean structure, but these will be ignored here, as they appear to be of second order in strength when compared to the nonlinear IWs in the PRIMER data.

The physical situation presented in the Shelfbreak PRIMER Experiment is more complex than any of the "simple" scattering cases for irregularly spaced propagating solitons, which are described to date in the acoustics literature. Because the study site encompassed the internal tide-generation region (at least some of the time) and included large bathymetric changes, the IW field underwent a distinct and complicated evolution over the 50-km cross-shelf extent of the PRIMER area [12]. Thus, we are faced with a physical situation that we are unable to fully model using even the best numerical oceanographic codes as input to the acoustics calculations. However, this does not preclude our trying to at least approximate the first-order physics of the scattering. So, in order to obtain a feeling for the effect of fine-scale oceanographic variability on acoustic propagation, this section looks at the results of a series of acoustic propagation runs made through a synthetic internal tide model based on the Korteweg–de Vries (KdV) equation (Colosi, private communication, [25]) and initialized using actual data.

The model used here for the evolution of the internal tide solibore was based on a modified version of the KdV equation. The model was initialized with a realistic solibore depression taken from thermistor data and then allowed to propagate for a 24-h period. Range-independent bathymetry and buoyancy frequency profiles were assumed. It should be noted that this particular KdV model does not include current shear and rotation effects, which can play important roles in determining the exact internal tide (Colosi, private communication).

The line plots in Fig. 24 show the resulting evolution of a single internal tidal bore over a 24-h period as it moves upslope. Tracking the leading edge of the internal tide disturbance yields a propagation velocity of around 0.7 m/s up the slope. The cycle repeats itself every 12.42 h, resulting in there being, at times, two internal tidal bores within the region between acoustic source and receiver. That situation will be considered, but only after understanding the effects of a single internal

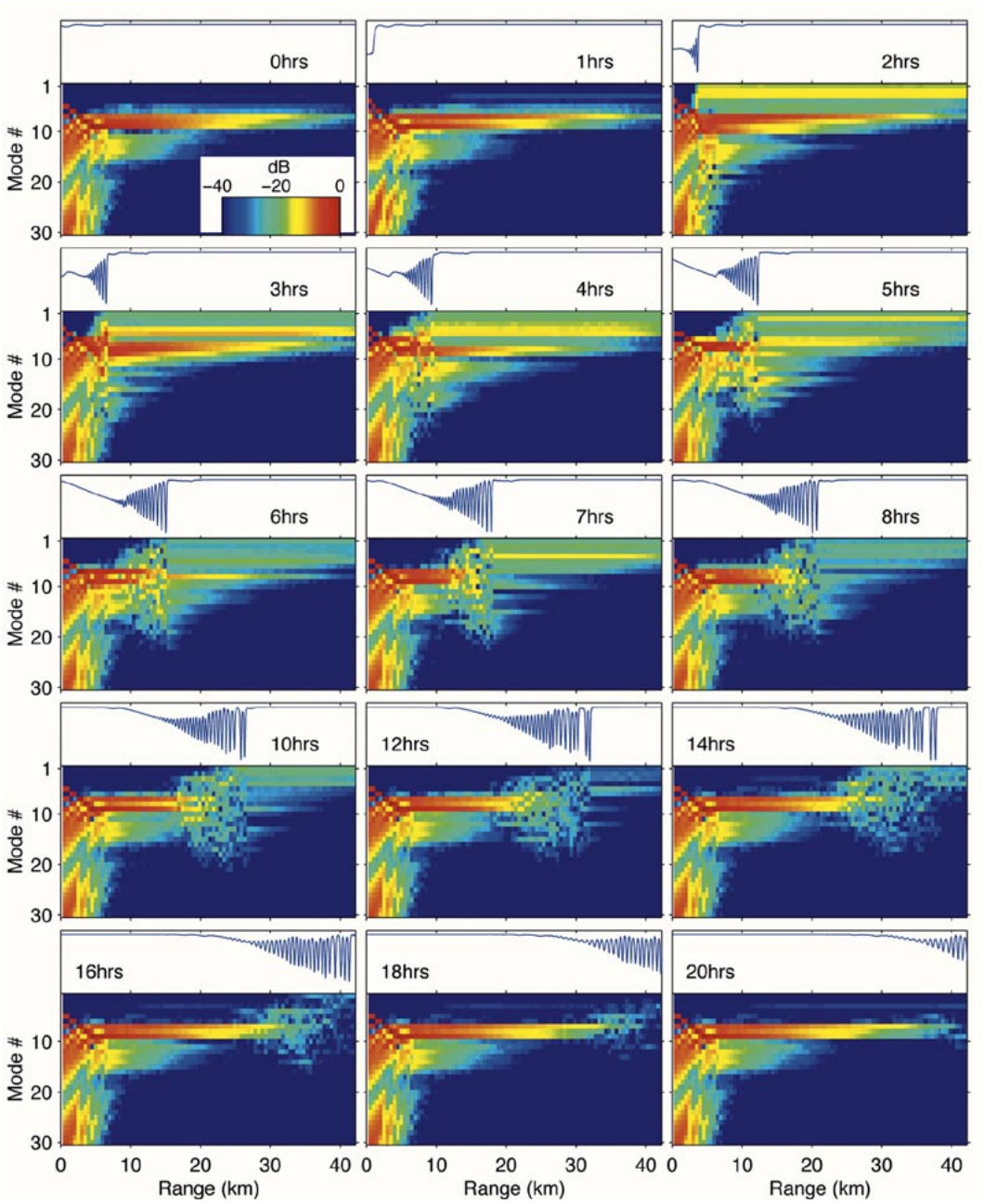

Fig. 24. Mode coupling due to an internal tide solibore over a 20-h period. Upper panels track the position and evolution of the solibore. Lower panels display mode amplitudes as a function of mode number and range.

solibore on acoustic propagation. Since the generation site of each internal tide cycle is difficult to place exactly, the initial bore depression used in this study has been shifted so that its leading edge is initially in line with the average generation site from Colosi *et al.* [12], which is also near the acoustic source location.

The model output shown in the blue and white panels of Fig. 24 is actually the KdV range solution times the amplitude of the first IW mode, which field data show is the dominant mode in the shelfbreak region. Using a representative depth profile for this first mode, the model output may then be easily converted into sound speed perturbations over depth, range, and time.

Parabolic equation calculations were then made through the ocean-model environment at half-hour intervals. To capture the rapid spatial variability of the solitons, very fine step sizes ($\Delta r = 1$ m) were used with the PE code. The generated pressure field was then projected onto the local mode shapes at a variety of ranges, as well as over the entire 100-Hz frequency band for selected ranges.

Fig. 24 also presents a series of color images showing how the acoustic mode amplitudes, as functions of mode number and range, are modified by the presence of an evolving solibore. It takes roughly 15 h for the leading edge of the solibore to reach the receiver from the source; a portion of the solibore tail still remains within the acoustic-propagation path even after 20 h, when the solibore leading edge has long since passed the receiver site. The obvious feature to note here is that, after passing through the solibore disturbance, the acoustic field has been

scattered into a much broader range of mode numbers than was found initially. Looking at the results after 6 h of model evolution, for example, modes 7 and 9 are initially the strongest near the acoustic source. At the 10-km range, energy is coupled into lower adjacent modes as the acoustic field transits the solibore. Modes 1 and 2 do not receive energy until the final coupling at the shock-like leading edge of the bore. However, at that point, the lowest modes *are* finally populated and, as there are always 1–2 solibores between the sources and receivers at the PRIMER site, it seems that we now understand the reason that we always have found substantial energy in the lowest modes in our acoustic data.

At the risk of redundancy, we will once more restate the argument that the last paragraph concludes. In Fig. 9, we show daily samples of data in which the lowest modes are populated. This is representative of the situation throughout the entire experiment. However, the range dependence of both the background water column SVP and the bathymetry (see Fig. 18) do not produce sufficient mode coupling to populate the lowest modes, as seen in Fig. 19. Fig. 21 shows that the shelfbreak front *can* produce enough coupling to populate the lowest modes, but only intermittently. However, as shown in Fig. 24, nonlinear IWs couple modes on a continuous basis, which finally explains the Fig. 9 results.

There are two practical points to be made with these simulations. The first is that the energy received in mode n at the VLA may have taken a variety of paths through mode space, depending on the configuration of the soliton field at that particular moment. This has important ramifications for the inverse problem, which relies (in current form) on predicting the unique mode travel paths. The second point, which was made before, is that there is now a clear mechanism for continuously getting high mode energy from a bottom-mounted source on the slope into the lower modes that are seen trapped in the cold-water duct on the shelf.

V. Conclusion

In this paper, we have examined the effects on point-to-point acoustics transmissions of the ocean bottom, the mesoscale oceanography, and the fine-scale oceanography. For the PRIMER experiment region of the NEB in summer conditions, one finds that the cross-shelf transmissions we examined are strongly mode coupled. One surprise, however, is that the bottom is not the strongest mode coupler in this region. Rather, the front (intermittently) and the nonlinear IWs (more steadily) are the largest contributors to range-dependent adiabatic and coupled mode behavior. Due to the foot of the shelfbreak front reducing the amount of bottom interaction, the oceanography actually tends to dominate the range dependence, which is *not* the usual case for shallow-water propagation.

Looking at the travel-time behavior of the acoustic normal modes, we see that the strong range dependence of the PRIMER site medium has led to the pulses being severely time spread, so that one cannot resolve individual modal arrivals. Rather, one is restricted to looking at the leading edge or centroid of a mode-filtered arrival (for any given mode). Thus, even if one regards the wander as independent of the spread (which it is not), one is left with only one independent data point for doing travel-time inverses for the medium sound speed. This makes the usual "adiabatic mode tomography" nonviable in regions such as the PRIMER site. Unless one can devise a fully coupled mode formalism, the use of tomography in such strong coupling regions is inadvisable.

Three-dimensional effects were also examined, both "acoustic and oceanographic." The out-of-plane acoustic-propagation effects were shown to be rather small for the upslope and diagonal-to-the-slope paths we examined. However, the three-dimensionality of the ocean IW field and, particularly, the east–west range dependence [12] impresses itself on both the spread and wander of the acoustics signal in a noticeable way, as seen by the difference between the upslope and diagonal-to-the-slope acoustic-propagation paths. This result reveals that even the fine-scale oceanography must be treated in a fully 3-D sense if one is to fully understand coastal acoustics transmissions.

Finally, it should be noted that this paper has treated only the eastern receiver receptions from the summer PRIMER experiment. A companion paper to this, treating the transmissions from the southeast and southwest sources to the northwest vertical array receiver in PRIMER is in preparation by Chiu *et al.*, which will extend the results found in this paper.

Appendix A

We will show the relative importance of the nonlinear versus the linear IWs in scattering sound in shallow water. In doing this, we will be presenting plausiblilty arguments based on several approximations. Thus, our results here will be indicative, but not absolute. Indeed, only a full numerical calculation including both the linear and nonlinear wave-scattering effects can fully answer the question of their relative importance for a given shallow-water waveguide. Nonetheless, some "rule of thumb" guidelines are still useful.

We assume a two-layer ocean model for the IWs, i.e., a less-dense thinner layer overlying a more-dense thicker layer. This is a simple model, but one that is not an unreasonable approximation for many shallow-water waveguides.

We will gauge "importance" by two effects that produce large amplitude fluctuations, specifically: 1) the mode coupling produced by the range dependence of the sound speed caused by the two species of IWs and 2) the change of the mode function at the source or receiver due to local IWs.

We first look at the mode coupling. In this case, we use the approximation that the mode coupling is proportional to the range derivative of the interface displacement of the two-layer IW field. (In our two-layer model, the density surface interface is also the sound speed field interface, so that the oceanographic variable tracks the acoustic one.) The proportionality of this derivative to the mode coupling for a three-layer IW model has already been shown by Preisig and Duda [26], so we do not feel that this approximation for two layers, which is a limiting case of theirs, is unreasonable. The use of this proportionality also follows the lead of S. Rutherford's 1979 Ph.D. thesis [27], in which he demonstrated that the usual mode-coupling integrals

could often be shown proportional to dc/dr for water column variability and dH/dr for bottom bathymetry variability.

For a nonlinear IW, a well-known solution to the Korteweg–deVries equation is the "sech-squared" wave, i.e., the interface displacement of our two layer system, $\eta(x)$ is

$$\eta(x) = A_{\rm sol}\mathrm{sech}^2(k_{\rm sol}x). \tag{1}$$

The range derivative of this expression is [see Preisig and Duda, (13)]

$$d\eta/dx = -2k_{\rm sol}A_{\rm sol}\mathrm{sech}^2(k_{\rm sol}x)\tanh(k_{\rm sol}x). \tag{2}$$

For the linear wave, we use a simple cosine wave, i.e.,

$$\eta(x) = A_{\rm lin}\cos(k_{\rm lin}x). \tag{3}$$

The derivative of this wave is a sine, i.e.,

$$d\eta/dx = -k_{\rm lin}A_{\rm lin}\sin(k_{\rm lin}x). \tag{4}$$

Thus, the ratio of (2) to (4) should give us the nonlinear-to-linear mode-coupling ratio. However, we can simplify this by noting that the sech, tanh, and sin functions are of order one and can be replaced by one for this estimation. This gives us a ratio R

$$R = \frac{2k_{\rm sol}A_{\rm sol}}{A_{\rm lin}k_{\rm lin}}. \tag{5}$$

What fraction of the range of the waveguide that is filled by the waves should also be factored in? This is 100% for linear waves, but more on the order of 50% for nonlinear waves (as the solibores have about 10-km wavelengths in PRIMER, but are spaced apart by about 20 km.) Thus, defining $f_{\rm sol}$ and $f_{\rm lin}$ as the fractions of the waveguide filled by each species of wave, we obtain

$$R = \frac{2k_{\rm sol}A_{\rm sol}f_{\rm sol}}{A_{\rm lin}k_{\rm lin}f_{\rm lin}}. \tag{6}$$

We can put some representative numbers into the above equation for the PRIMER experiment. Typical wavelengths $\lambda = 2\pi/k$ are 300 m for the solitons and 1000 m for the linear waves. Typical amplitudes are 5 m for the solitons and 2.5 m for the linear waves. Finally, the fractional factors are as discussed above. Putting these numbers into our equation yields a nonlinear-to-linear coupling ratio of about seven, clearly indicating that nonlinear effects dominate for this process.

We next consider the change in the mode amplitudes due to the local IWs. For this process, we make the assumption that the change in the local modefunction is proportional to the amplitude of the local IW depression of the interface layer. This is not strictly true, as the dependence of the mode function on the sound speed profile perturbation is a nonlinear one. However, as a crude first approximation, we will linearize this and see where it takes us. Using the above equations for the amplitudes and again incorporating the fraction of the range occupied, we simply get

$$R = \frac{A_{\rm sol}f_{\rm sol}}{A_{\rm lin}f_{\rm lin}}. \tag{7}$$

For the numbers we used previously, this gives a ratio of unity, i.e., both types of waves should be equally important. However, this result may be questionable due to our linearization assumption. Moreover, numerical calculations using parabolic equation models inputting reasonable linear and nonlinear IW fields showed that the linear waves had almost negligible impact as compared to the nonlinear waves in the PRIMER region.

ACKNOWLEDGMENT

The authors would like to thank their former ONR program managers, Dr. J. Simmen and Dr. L. Goodman, for both their financial and personal support for this project. They also thank the WHOI SeaSoar Group, including P. Fucile, F. Bahr, A. Gordon, J. Dean, and E. Levy for their outstanding work at sea, including the development of a completely reliable bottom-avoidance system. They also thank the WHOI Buoy Engineering Lab personnel, especially J. Kemp and L. Costello, for their usual superb job. The captain and crew of the *R/V Endeavor* provided excellent support throughout the cruise, as well as cheerful companionship at the Captain Kidd and the Leeside taverns. Finally, they thank J. Colosi of WHOI for his KdV calculations and helpful discussions. This is WHOI Contribution Number 10 947.

REFERENCES

[1] G. Jin, J. F. Lynch, C.-S. Chiu, and J. H. Miller, "A theoretical and simulation study of acoustic normal mode coupling effects due to the barents sea polar front, with applications to acoustic tomography and matched-field processing," *J. Acoust. Soc. Amer.*, vol. 100, no. 1, pp. 193–205, July 1996.

[2] J. R. Apel, M. Badiey, C. S. Chiu, S. Finette, R. Headrick, J. Kemp, J. Lynch, A. Newhall, M. Orr, B. H. Pasewark, D. Tielburger, A. Turgut, K. von der Heydt, and S. Wolf, "An overview of the 1995 SWARM shallow-water internal wave acoustic scattering experiment," *IEEE J. Oceanic Eng.*, vol. 22, pp. 465–500, July 1997.

[3] C.-S. Chiu, J. H. Miller, and J. F. Lynch, "Forward coupled-mode propagation modeling for coastal acoustic tomography," *J. Acoust. Soc. Amer.*, vol. 99, pp. 793–802, Feb. 1996.

[4] J. F. Lynch, G. Jin, R. Pawlowicz, D. Ray, A. Plueddemann, C.-S. Chiu, J. H. Miller, R. H. Bourke, A. R. Parsons, and R. Muench, "Acoustic travel-time perturbations due to shallow-water internal waves and internal tides in the barents sea polar front: Theory and experiment," *J. Acoust. Soc. Amer.*, vol. 99, pp. 803–821, Feb. 1996.

[5] R. H. Headrick and J. F. Lynch, "Acoustic normal mode fluctuation statistics in the 1995 SWARM internal wave scattering experiment," *J. Acoust. Soc. Amer.*, vol. 107, no. 1, pp. 201–220, 2000.

[6] ——, "Modeling mode arrivals in the 1995 SWARM experiment acoustic transmissions," *J. Acoust. Soc. Amer.*, vol. 107, no. 1, pp. 221–236, 2000.

[7] S. Finette, M. H. Orr, A. Turgut, and J. R. Apel, "Acoustic field variability induced by time-evolving internal wave fields," *J. Acoust. Soc. Amer.*, vol. 108, no. 3, pp. 957–972, 2000.

[8] J. F. Lynch, A. Newhall, B. Sperry, G. Gawarkiewicz, A. Fredricks, P. Tyack, C. S. Chiu, and P. Abbot, "Spatial and temporal variations in acoustic propagation characteristics at the New England shelfbreak front," *IEEE J. Oceanic Eng.*, vol. 28, pp. 129–150, Jan. 2003.

[9] C. A. Linder and G. Gawarkiewicz, "A climatology of the shelfbreak front in the Middle Atlantic Bight," *J. Geophys. Res.*, vol. 103, no. C9, pp. 18 405–18 423, 1998.

[10] J. F. Lynch, A. Newhall, C. S. Chiu, and J. H. Miller, "Ocean prediction and acoustic propagation models," in *Three Dimensional Ray Acoustics in a Realistic Ocean*. New York: AIP, 1994, pp. 198–232. Series in Modern Acoustics and Signal Processing.

[11] G. Gawarkiewicz, F. Bahr, K. Brink, M. Caruso, J. Lynch, and C. S. Chiu, "A large-amplitude meander of the shelfbreak front south of New England: Observations from the Shelfbreak PRIMER Experiment," J. Geophys. Res., 2003, submitted for publication.

[12] J. A. Colosi, J. F. Lynch, R. C. Beardsley, G. Gawarkiewicz, A. Scotti, and C.-S. Chiu, "Observations of nonlinear internal waves on the New England continental shelf during the summer shelfbreak PRIMER," *J. Geophys. Res.*, vol. 106, no. C5, pp. 9587–9601, 2001.
[13] C. Garrett and W. Munk, "Space-time scales of internal waves," *Geophys. Fl. Dynam.*, vol. 2, pp. 225–264, 1972.
[14] B. S. Racine, "A Characterization of Internal Solitons in the SWARM Region of the New York Bight," Master's Thesis, Massachusetts Inst. Technol./Woods Hole Oceanographic Inst., Aug. 1996.
[15] G. R. Potty, J. H. Miller, and J. F. Lynch, "Inversion for sediment geoacoustic properties at the New England Bight," J. Acoust. Soc. Amer., 2003, to be published.
[16] R. H. Headrick, "Analysis of Internal Wave Induced Mode Coupling Effects on the 1995 SWARM Acoustic Transmissions," Ph.D. Thesis, Massachussetts Inst. Technol./Woods Hole Oceanographic Inst., June 1997.
[17] B. J. Sperry, "Analysis of Acoustic Propagation in the Region of the New England Continental Shelfbreak," Ph.D. Thesis, Massachussetts Institute of Technology/Woods Hole Oceanographic Institution, June 1999.
[18] M. D. Collins, "User's Guide for RAM Versions 1.0 and 1.0p," Naval Research Laboratory, Washington, D.C., Tech. Rep., 1994.
[19] M. Porter, "The KRAKEN Normal Mode Program," SACLANTCEN, La Spezia, Italy, Tech. Rep. SM-245, 1991.
[20] A. F. Richards, "Atlantic Margin Coring Project 1976-Preliminary Report on Shipboard and Some Laboratory Geotechnical Data," U.S. Geol. Surv., Open File Rep. 78-123, 1977.
[21] H. Medwin and C. S. Clay, *Fundamentals of Acoustical Oceanography*. New York: Academic, 1998.
[22] L. M. Brekhovskikh and Y. P. Lysanov, *Fundamentals of Ocean Acoustics*, 2nd ed. Berlin, Germany: Springer-Verlag, 1990.
[23] H. Weinberg and R. Burridge, "Horizontal ray theory for ocean acoustics," *J. Acoust. Soc. Amer.*, vol. 55, no. 1, pp. 63–78, 1974.
[24] F. S. Henyey and H. Antje, "Energetics of borelike internal waves," *J. Geophys. Res.*, vol. 102, no. C2, pp. 3323–3330, 1997.
[25] J. R. Apel, L. A. Ostrovsky, and Y. A. Stepanyants, "Internal Solitons in the Ocean," Applied Physics Laboratory: The Johns Hopkins University, Tech. Rep. MERCJRA0695, July 1995.
[26] J. C. Preisig and T. F. Duda, "Coupled acoustic mode propagation through continental-shelf internal solitary waves," *IEEE J. Oceanic Eng.*, vol. 22, pp. 256–269, Apr. 1997.
[27] S. R. Rutherford, "An Examination of Coupled Mode Theory as Applied to Underwater Sound Propagation," Ph.D. Thesis, University of Texas, Austin, TX, Aug. 1979.

Brian J. Sperry received the B.S. degree in electrical engineering from the University of Iowa, Iowa City, in 1990 and the S.M. and Ph.D. degrees from the Massachusetts Institute of Technology (MIT), Cambridge, and Woods Hole Oceanographic Institution (WHOI), Woods Hole, MA, joint program in oceanographic engineering in 1994 and 1999, respectively.

He is with Science Applications International Corporation (SAIC), McLean, VA, as a Senior Scientist in the Ocean Sciences Division. His research interests include acoustical oceanography, underwater acoustics, and array processing.

Dr. Sperry is a Member of the Acoustical Society of America.

James F. Lynch (M'96–SM'03) was born in Jersey City, NJ, on June 3, 1950. He received the B.S. degree in physics from Stevens Institute of Technology, Newark, NJ, in 1972 and the Ph.D. degree in physics from the University of Texas at Austin in 1978.

He was with the Applied Research Laboratories, University of Texas at Austin (ARL/UT), from 1978 to 1981, after which he joined the scientific staff at the Woods Hole Oceanographic Institution (WHOI), Woods Hole, MA. He has been with WHOI since then and currently holds the position of Senior Scientist in the Applied Ocean Physics and Engineering Department. His research specialty areas are ocean acoustics and acoustical oceanography, but he also greatly enjoys occasional forays into physical oceanography, marine geology, and marine biology.

Dr. Lynch is a Fellow of the Acoustical Society of America and the Editor-in-Chief of the IEEE JOURNAL OF OCEANIC ENGINEERING.

Glen Gawarkiewicz was born in Staten Island, NY, in 1959. He received the B.S. degree in ocean engineering from Massachusetts Institute of Technology (MIT), Cambridge, in 1981 and the Ph.D. degree from the University of Delaware, Newark, in physical oceanography in 1989.

He has been with the Woods Hole Oceanographic Institution since 1989, where he is presently an Associate Scientist. His research interests include frontal dynamics, particularly of shelfbreak regions, as well as continental shelf processes in general. He is also interested in the effect of oceanographic processes on acoustics.

Ching-Sang Chiu received the Ph.D. degree from the Massachusetts Institute of Technology (MIT), Cambridge, and Woods Hole Oceanographic Institution (WHOI), Woods Hole, MA, joint program in 1985.

He is Professor of Oceanography at the Naval Postgraduate School. His current research interests include shallow-water acoustics, particularly volume variability effects in shelfbreak regions; coastal ocean acoustic tomography; and passive detection and censusing of marine mammal vocalizations.

Dr. Chiu is a Fellow of the Acoustical Society of America.

Arthur Newhall received the B.S. degree in mathematics from the University of Maine, Orono, in 1985.

He is a Research Specialist in the Applied Ocean Physics and Engineering Department, Woods Hole Oceanographic Institution, Woods Hole, MA. His current research interests include ocean acoustic-propagation modeling, acoustical oceanography, ocean acoustic tomography, and software engineering.